

### III. 研究成果の刊行に関する一覧表

研究成果の刊行に関する一覧表

雑誌

発表者氏名	論文タイトル名	発表誌名	巻号	ページ	出版年
Yamada S., Kubo Y., Yamazaki D., Sekino Y., Kanda Y.	Chlorpyrifos inhibits neural induction via Mfn1-mediated mitochondrial dysfunction in human induced pluripotent stem cells.	Sci. Rep.	7	40925	2017
Yamada S., Asanagi M., Hirata N., Itagaki H., Sekino Y., Kanda Y.	Tributyltin induces mitochondrial fission through Mfn1 degradation in human induced pluripotent stem cells.	Toxicol. In Vitro.	34	257-263	2016
Asanagi M., Yamada S., Hirata N., Itagaki H., Kotake Y., Sekino Y., Kanda Y.	Tributyltin induces G2/M cell cycle arrest via NAD(+)-dependent isocitrate dehydrogenase in human embryonic carcinoma cells.	J. Toxicol. Sci.	41	207-215	2016
Hirata N., Yamada S., Asanagi M., Sekino Y., Kanda Y.	Nicotine induces mitochondrial fission through mitofusin degradation in human multipotent embryonic carcinoma cells.	Biochem. Biophys. Res. Commun.	470	300-305	2016
Mabuchi H., Ong HY, Watanabe K., Yoshida S., Hozumi N.	Visualization of Spatially Distributed Bioactive Molecules Using Enzyme-Linked Photo Assay.	IEEJ Transactions on Fundamentals and Materials	136	99-104	2016
Ishidao T., Fueta Y., Ueno S., Yoshida Y., Hori H.	A cross-fostering analysis of bromine ion concentration in rats that inhaled 1-bromopropane vapor.	J Occup Health	58	241-246	2016
Fueta Y., Sekino Y., Yoshida S., Kanda Y., Ueno S.	Prenatal exposure to valproic acid alters the development of excitability in the postnatal rat hippocampus.	論文投稿中			
Fueta Y., Ishidao T., Ueno S., Yoshida Y., Kanda Y., Hori H.	Prenatal exposure to 1-bromopropane causes delayed adverse effects on hippocampal neuronal excitability in the CA1 subfield of rat offspring.	論文投稿中			
Igarashi T., Wilson DJ., Ueno S.	Acute exposure to toluene and xylene decrease the expression of connexin43 in human cardiac myocytes.	論文投稿中			
Kasuga Y., Hata K., Tajima A., Ochiai D., Saisho Y., Matsumoto T., Arata N., Miyakoshi K., Tanaka M.	Association of common polymorphisms with gestational diabetes mellitus in Japanese women: A case-control study.	Endocr J. in press			
Sakaki M., Ebihara Y., Okamura K., Nakabayashi K., Igarashi A., Matsumoto K., Hata K., Kobayashi Y., Maehara K.	Potential roles of DNA methylation in the initiation and establishment of replicative senescence revealed by array-based methylome and transcriptome analyses.	PLoS One.	12	e0171431	2017

Liao H., Sato H., Chiba R., Kawai T., Nakabayashi K., Hata K., Akutsu H., Fujiwara S., Nakamura H.	Human cytomegalovirus downregulates SLITRK6 expression through IE2.	J Neurovirol.	23	79-86	2017
Ito Y., Maehara K., Kaneki E., Matsuoka K., Sugahara N., Miyata T., Kamura H., Yamaguchi Y., Kono A., Nakabayashi K., Migita O., Higashimoto K., Soejima H., Okamoto A., Nakamura H., Kimura T., Wake N., Taniguchi T., Hata K.	Novel Nonsense Mutation in the NLRP7 Gene Associated with Recurrent Hydatidiform Mole.	Gynecol Obstet Invest.	81	353-358	2016
Nohara K., Okamura K., Suzuki T., Murai H., Ito T., Shinjo K., Takumi S., Michikawa T., Kondo Y., Hata K.	Augmenting effects of gestational arsenite exposure of C3H mice on the hepatic tumors of the F2 male offspring via the F1 male offspring.	J Appl Toxicol.	36	105-112	2016

#### IV. 研究成果の刊行物・別刷

Original Article

# Tributyltin induces G2/M cell cycle arrest via NAD<sup>+</sup>-dependent isocitrate dehydrogenase in human embryonic carcinoma cells

Miki Asanagi<sup>1,2,\*</sup>, Shigeru Yamada<sup>1,\*</sup>, Naoya Hirata<sup>1</sup>, Hiroshi Itagaki<sup>2</sup>, Yaichiro Kotake<sup>3</sup>,  
Yuko Sekino<sup>1</sup> and Yasunari Kanda<sup>1</sup>

<sup>1</sup>Division of Pharmacology, National Institute of Health Sciences

<sup>2</sup>Faculty of Engineering, Department of Materials Science and Engineering, Yokohama National University

<sup>3</sup>Department of Xenobiotic Metabolism and Molecular Toxicology, Graduate School of Biomedical and Health Sciences, Hiroshima University

(Received November 16, 2015; Accepted December 28, 2015)

**ABSTRACT** — Organotin compounds, such as tributyltin (TBT), are well-known endocrine-disrupting chemicals (EDCs). We have recently reported that TBT induces growth arrest in the human embryonic carcinoma cell line NT2/D1 at nanomolar levels by inhibiting NAD<sup>+</sup>-dependent isocitrate dehydrogenase (NAD-IDH), which catalyzes the irreversible conversion of isocitrate to  $\alpha$ -ketoglutarate. However, the molecular mechanisms by which NAD-IDH mediates TBT toxicity remain unclear. In the present study, we examined whether TBT at nanomolar levels affects cell cycle progression in NT2/D1 cells. Propidium iodide staining revealed that TBT reduced the ratio of cells in the G1 phase and increased the ratio of cells in the G2/M phase. TBT also reduced cell division cycle 25C (*cdc25C*) and cyclin B1, which are key regulators of G2/M progression. Furthermore, apigenin, an inhibitor of NAD-IDH, mimicked the effects of TBT. The G2/M arrest induced by TBT was abolished by NAD-IDH $\alpha$  knockdown. Treatment with a cell-permeable  $\alpha$ -ketoglutarate analogue recovered the effect of TBT, suggesting the involvement of NAD-IDH. Taken together, our data suggest that TBT at nanomolar levels induced G2/M cell cycle arrest via NAD-IDH in NT2/D1 cells. Thus, cell cycle analysis in embryonic cells could be used to assess cytotoxicity associated with nanomolar level exposure of EDCs.

**Key words:** Embryonic carcinoma cells, Tributyltin, Cell cycle, Isocitrate dehydrogenase

## INTRODUCTION

Organotin compounds, such as tributyltin (TBT) are typical environmental contaminants and are categorized as endocrine-disrupting chemicals (EDCs), which cause neurodevelopmental defects including behavioral abnormality and teratogenicity (Dopp *et al.*, 2004; Gårdlund *et al.*, 1991). Although the use of TBT has already been restricted, butyltin compounds, including TBT, can still be found in human blood at concentrations between 50 and 400 nM. There is still concern about TBT toxicity for human health (Whalen *et al.*, 1999).

Several studies have revealed that TBT activates retinoid X receptor (RXR) and/or peroxisome proliferator-activated receptor  $\gamma$  (PPAR $\gamma$ ) (Kanayama *et al.*, 2005). TBT

at nanomolar levels has the ability to bind with higher affinity than the intrinsic ligands and these genomic transcriptional activations have been reported to mediate neurodevelopmental defects in *Xenopus* (Yu *et al.*, 2011). In contrast, TBT elicits non-genomic pathway in mature rat neurons and brain tissues at nearly micromolar levels. For instance, TBT induces neuronal death by inhibiting mammalian target of rapamycin (mTOR) in rat cortical neurons (Nakatsu *et al.*, 2010). TBT also induces neuronal degeneration via the generation of reactive oxygen species along with marked reduction of GSH/GSSG levels in the rat brain (Mitra *et al.*, 2013).

Cell stress is known to trigger a checkpoint that arrests cells in the G1 or G2 phase (Gabrielli *et al.*, 2012). The cell cycle is tightly regulated by spatial and temporal

Correspondence: Yasunari Kanda (E-mail: kanda@nihs.go.jp)

\*These authors equally contributed to this work.

expression of cell cycle proteins and divided into p53-dependent and p53-independent regulations (Shackelford *et al.*, 1999). In the p53-independent regulations, cdc25C phosphatase, a mitotic inducer, plays a central role in G2/M phase regulation. Cdc25C activates cyclin B1/cyclin-dependent kinase (Cdk) 1 complex, which triggers mitosis (Donzelli and Draetta, 2003) and cyclin B1 accumulates during the S and G2 phases, followed by nuclear translocation and association with Cdk1. Protein levels of these cell cycle regulators are strictly regulated during cell cycle progression. Ultraviolet irradiation or toxic drugs are known to cause G2 arrest by the inactivation of cyclin B1/Cdk1 via p53 induction followed by the upregulation of p21, a Cdk inhibitor and/or cdc25C downregulation by degradation (Chaudhary *et al.*, 2013; Kawabe, 2004; Nam *et al.*, 2010; Ouyang *et al.*, 2009).

We have previously reported that nanomolar levels of TBT induce growth arrest of neuronal precursor NT2/D1 cells as a model of neurodevelopmental stage (Yamada *et al.*, 2013). We found that TBT causes growth arrest via mitochondrial NAD<sup>+</sup>-dependent isocitrate dehydrogenase (NAD-IDH), which catalyzes the irreversible conversion of isocitrate to  $\alpha$ -ketoglutarate in the tricarboxylic acid (TCA) cycle (Yamada *et al.*, 2014). Based on these observations, we hypothesized that nanomolar levels of TBT could also affect cell cycle progression via NAD-IDH in NT2/D1 cells.

In the present study, we investigated the effect of TBT on cell cycle progression in NT2/D1 cells. We found that exposure to 100 nM TBT reduced the protein levels of cell cycle regulators and induced G2/M cell cycle arrest through an NAD-IDH-dependent mechanism. Thus, cell cycle regulation via NAD-IDH is a novel target of TBT-induced toxicity in human embryonic carcinoma cells.

## MATERIALS AND METHODS

### Cell culture

NT2/D1 cells were obtained from the American Type Culture Collection (Manassas, VA, USA). The cells were cultured in Dulbecco's modified Eagle's medium (DMEM; Sigma-Aldrich, St. Louis, MO, USA) supplemented with 10% fetal bovine serum (FBS; Biological Industries, Ashrat, Israel) and 0.05 mg/mL penicillin-streptomycin mixture (Life Technologies, Carlsbad, CA, USA) at 37°C in 5% CO<sub>2</sub>.

### Cell cycle analysis

The cells were trypsinized and harvested in phosphate buffered saline. Then the cells were resuspended in 70% ethanol for 30 min at -20°C. The fixed cells were collected

by centrifugation and resuspended in propidium iodide (PI)/RNase Staining Buffer (BD Biosciences, San Jose, CA, USA) followed by incubation at room temperature for 30 min in the dark. Cell cycle distribution was determined by flow cytometric analysis of the DNA content using the BD FACS Aria II system (BD Biosciences). Data were analyzed by Modfit LT 4.0 (Verity Software House, Topsham, ME, USA).

### Real-time PCR

Total RNA was extracted from NT2/D1 cells using TRIzol reagent (Life Technologies), and quantitative real-time reverse transcription (RT)-PCR was performed with QuantiTect SYBR Green RT-PCR Kit (QIAGEN, Valencia, CA, USA) using an ABI PRISM 7900HT sequence detection system (Applied Biosystems, Foster City, CA, USA) as previously reported (Hirata *et al.*, 2014). The relative change in transcript amounts was normalized to the expression levels of glyceraldehyde-3-phosphate dehydrogenase (GAPDH). The following primer sequences were used for real-time PCR analysis: human cdc25C: forward, 5'-AGGCAGCCTTGAGTTGCATAGAGA-3', reverse, 5'-AGAGTTGGCTGGCTTGTGAGAAGA-3'; humancyclin B1: forward, 5'-CGGGAAGTCACTGGAAACAT-3', reverse, 5'-AAACATGGCAGTGACACCAA-3'; human GAPDH: forward, 5'-GTCTCCTCTGACTTCAACAGCG-3', reverse, 5'-ACCACCCTGTTGCTGTAGCCAA-3'.

### Western blot analysis

Western blot analysis was performed as previously reported (Kanda *et al.*, 2011). Briefly, cells were lysed with Cell Lysis Buffer (Cell Signaling Technology, Danvers, MA, USA). The proteins were then separated by sodium dodecyl sulfate-polyacrylamide gel electrophoresis (SDS-PAGE) and electrophoretically transferred to Immobilon-P membrane (Millipore, Billerica, MA, USA). The membranes were probed with an anti-cdc25C monoclonal antibody (1:1,000; Cell Signaling Technology), an anti-cyclin B1 monoclonal antibody (1:1,000; Cell Signaling Technology), and an anti-GAPDH polyclonal antibody (1:2,500; Abcam, Cambridge, UK) followed by incubation with horseradish peroxidase-conjugated secondary antibodies against rabbit or mouse IgG (Cell Signaling Technology). The bands were visualized using the ECL Western Blotting Analysis System (GE Healthcare, Buckinghamshire, UK), and images were acquired using a LAS-3000 Imager (FUJIFILM UK Ltd., Systems, Bedford, UK).

### NAD-IDH activity assay

NAD-IDH activity was determined using the

## TBT induces G2/M cell cycle arrest in human embryonic carcinoma

Isocitrate Dehydrogenase Activity Colorimetric Assay Kit (Biovision, Mountain View, CA, USA), according to the manufacturer's instructions. Briefly, NT2/D1 cells were lysed in an assay buffer provided in the kit. The lysate was centrifuged at 14,000 *g* for 15 min, and the cleared supernatant was used for the assay.

### NAD-IDH $\alpha$ knockdown

Knockdown studies were performed using NAD-IDH $\alpha$  shRNA lentiviruses from Sigma-Aldrich (MISSION shRNA) according to the manufacturer's protocol. A scrambled hairpin sequence was used as a negative control. Briefly, the cells were infected with the viruses at a multiplicity of infection of 10 in presence of 8  $\mu$ g/mL hexadimethrine bromide (Sigma-Aldrich) for 24 hr, and were then subjected to selection with 0.5  $\mu$ g/mL puromycin for 72 hr for further functional analyses.

### Chemicals and reagents

Tributyltin Chloride was obtained from Tokyo Chemical Industry (Tokyo, Japan). Tin acetate (TA), apigenin, and dimethyl  $\alpha$ -ketoglutarate (DMKG) were obtained from Sigma-Aldrich.

### Statistical analysis

All data were presented as mean  $\pm$  S.D. Analysis of variance (ANOVA) followed by post hoc Tukey's test was used to analyze the data in Figs. 1C, 1D, 1E, 2A, 2B, 3C, 4E, 5A, 5B, 6A and 6B. Student's *t* test was used to analyze the data in Figs. 3A, 3B, 4A, 4B and 4C. P-values less than 0.05 were considered to be statistically significant.

## RESULTS

### Effect of TBT on cell cycle progression

We have previously found that 100 nM TBT induced growth arrest in NT2/D1 cells (Yamada *et al.*, 2013). Here we investigated whether TBT affects cell cycle progression. Exposure to 100 nM TBT for 48 hr decreased the proportion of cells in the G1 phase (51.9% decrease) and increased of the proportion of cells in the G2/M phase (79.6% increase), compared with untreated control cells (Figs. 1A-E). In contrast, TBT did not affect the proportion of cells in the S phase. Moreover, exposure to tin acetate (TA), which is less toxic, did not affect cell cycle progression. These data suggest that TBT induces G2/M cell cycle arrest in the cells.

### TBT exposure reduces G2/M cell cycle regulators, cdc25C and cyclin B1

To examine the molecular mechanism by which TBT

induces G2/M cell cycle arrest, we assessed the protein levels of p53, a major cell cycle regulator. We found that p53 protein level was reduced after 24 hr of TBT treatment, whereas cisplatin, which is known to cause p53-dependent G2/M cell cycle arrest (Pani *et al.*, 2007), increased p53 levels (Supplementary Fig. 1). Since we could not observe p53-dependency in TBT-induced G2/M cell cycle arrest, we assessed cdc25C and its downstream factor, cyclin B1, which are also involved in G2/M progression of cell cycle. Western blot analysis revealed that cdc25C and cyclin B1 protein levels were reduced after 24 hr of TBT treatment (Fig. 2A). In contrast, exposure to TA did not affect cdc25C and cyclin B1 protein levels. Equal GAPDH protein expression levels were confirmed as a loading control. Next, we assessed the gene expression of cdc25C and cyclin B1. However, real-time PCR analysis showed that gene expression was not significantly altered by TBT exposure for both 24 and 48 hr (Fig. 2B). These data suggest that TBT-induced G2/M cell cycle arrest is caused by reduction of cdc25C and cyclin B1 proteins.

### TBT induces G2/M cell cycle arrest via NAD-IDH

To investigate the molecular mechanisms by which cdc25C is degraded and G2/M cell cycle arrest is induced, we examined the effect of the PPAR $\gamma$  agonist rosiglitazone (RGZ), which is the genomic target of TBT. We found that RGZ did not induce G1 phase reduction and G2/M phase increase (Figs. 3A and B). RGZ at 100 nM induced PPAR $\gamma$  gene expression at similar level to 100 nM TBT in NT2/D1 cells (Fig. 3C), confirming the agonistic effect of RGZ on PPAR $\gamma$  expression described in previous report (Benkirane *et al.*, 2006). These data suggest that TBT induces G2/M cell cycle arrest in NT2/D1 cells through a non-genomic pathway. We next examined the involvement of the non-genomic target NAD-IDH. We used an NAD-IDH inhibitor apigenin (Arango *et al.*, 2013) at 10  $\mu$ M, which reduced NAD-IDH activity to a level (22.4%) (Fig. 4A). As previously reported, 100 nM TBT had a similar inhibitory effect (24.4%; Yamada *et al.*, 2014). Treatment with apigenin (10  $\mu$ M, 48 hr) decreased G1 phase ratio (58.6% decrease) and increased G2/M phase ratio (98.1% increase) (Figs. 4B and C). Similar to TBT, apigenin reduced protein expression of cdc25C and cyclin B1 without affecting gene expression (Figs. 4D and E). To further confirm the effect of apigenin, we performed knockdown (KD) experiments of NAD-IDH $\alpha$ , the catalytic subunit of NAD-IDH, using lentivirus-delivered shRNAs. Real-time PCR analysis showed that KD efficiency was approximately 40% (Yamada *et al.*, 2014). We could not obtain more highly KD cells because of cell

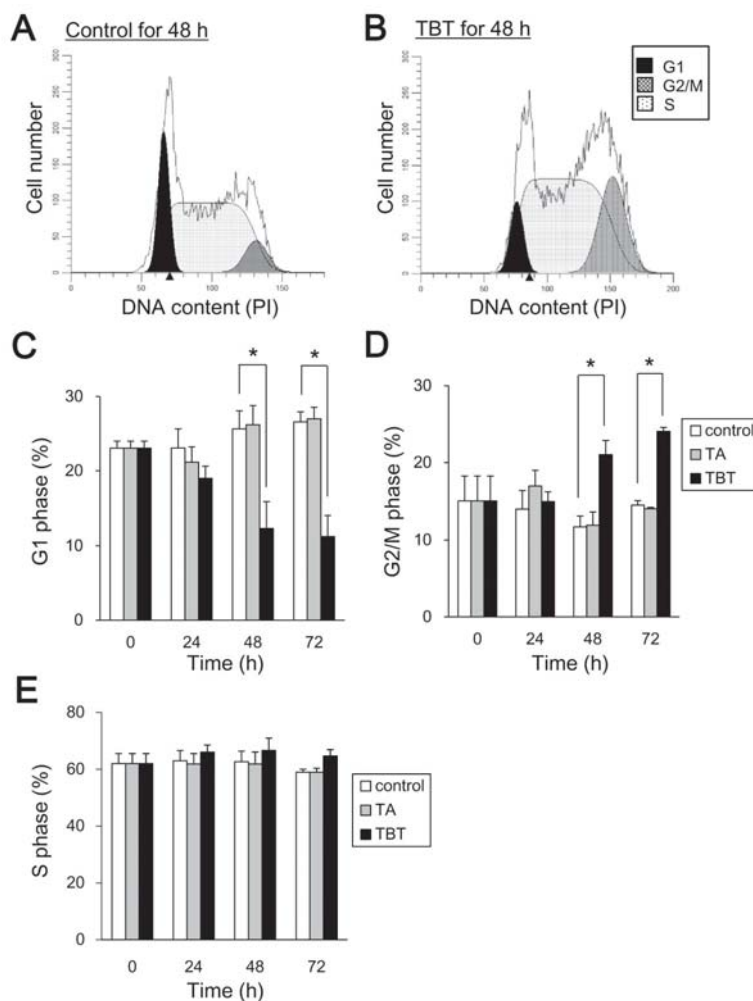


**Fig. 1.** Effect of TBT on cell cycle progression in NT2/D1 cells. Cells were exposed to 100 nM TA or TBT for 24, 48 or 72 hr. Cells were stained with propidium iodide (PI). Cell cycle distribution was determined by flow cytometric analysis of the DNA content on BD FACS Aria II. Representative cell cycle data in control (A) and TBT (B)-treated cells. The area ratio of G1 (C), G2/M (D) and S (E) phases was determined by Modfit LT 4.0. Data represent mean  $\pm$  S.D. (n = 3). \*P < 0.05.

death. Due to partial KD of the NAD-IDH $\alpha$  gene, NAD-IDH activity decreased by 22%, which is comparable to its decreased levels by TBT. In our previous studies, we observed that NAD-IDH $\alpha$  KD recovered the inhibitory effect of TBT on ATP content (Yamada *et al.*, 2014). This might be because the TBT target NAD-IDH $\alpha$  was already inhibited by shRNA and further inhibition by TBT was not observed in the knockdown cells. Similar to these data, NAD-IDH $\alpha$  KD abolished the TBT-induced G1 phase reduction and G2/M phase increase (Figs. 5A and B), suggesting the involvement of NAD-IDH on TBT effects. NAD-IDH $\alpha$  KD tended to decrease the proportion of cells in the G1 phase (24.1%  $\pm$  0.55 to 23.2%  $\pm$  0.34) and

increase the proportion of cells in the G2/M phase (17.5%  $\pm$  1.6 to 20.3%  $\pm$  0.62), compared with control (Figs. 5A and B). Moreover, NAD-IDH $\alpha$  KD also abolished the TBT-induced reduction of cdc25C and cyclin B1 proteins (Fig. 5C). NAD-IDH $\alpha$  KD reduced the basal levels of cdc25C and cyclin B1 proteins, compared with control (Fig. 5C). These data suggest that NAD-IDH mediates TBT-induced G2/M cell cycle arrest in NT2/D1 cells. To further confirm the involvement of NAD-IDH, we treated the cells with dimethyl  $\alpha$ -ketoglutarate (DMKG), a cell-permeable analog of  $\alpha$ -ketoglutarate (Willenborg *et al.*, 2009). Incubation with DMKG prevented TBT-induced G2/M cell cycle arrest in NT2/D1 cells and

TBT induces G2/M cell cycle arrest in human embryonic carcinoma

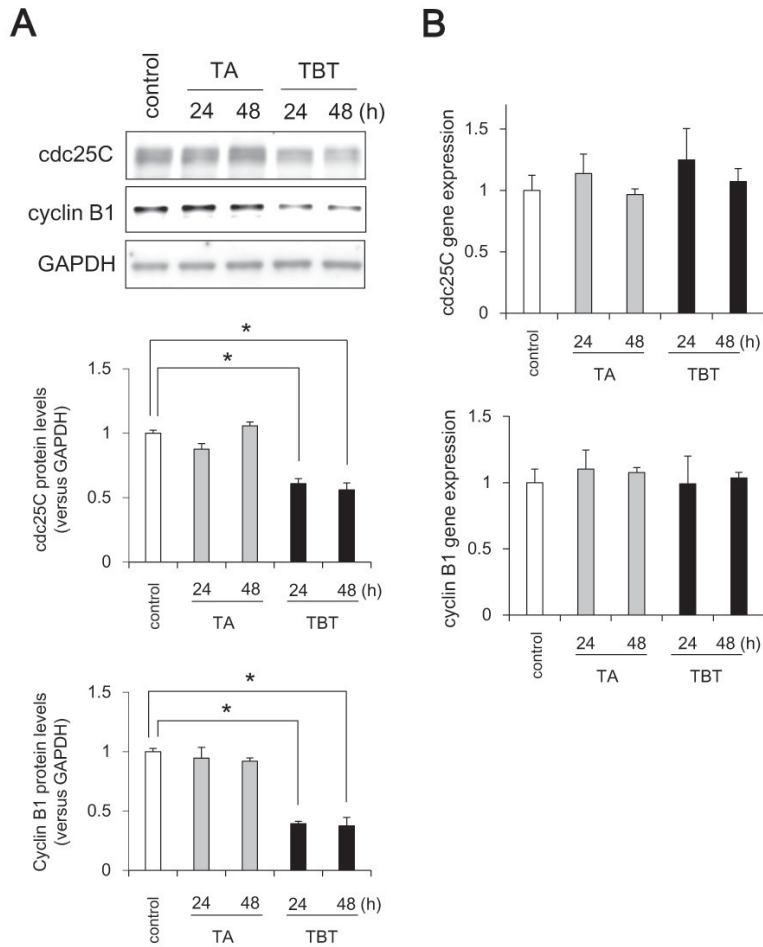


**Fig. 2.** Effect of TBT on expression levels of G2/M cell cycle regulators in NT2/D1 cells. After TBT exposure for 24 and 48 hr, protein expression was analyzed by western blot using anti-cdc25C, cyclin B1, or GAPDH antibodies (A). After TBT exposure for 24 or 48 hr, the expression of G2/M cell cycle regulators was analyzed by real time PCR (B). The gene expression was not significantly altered by TBT exposure. Data represent mean  $\pm$  S.D. (n = 3).

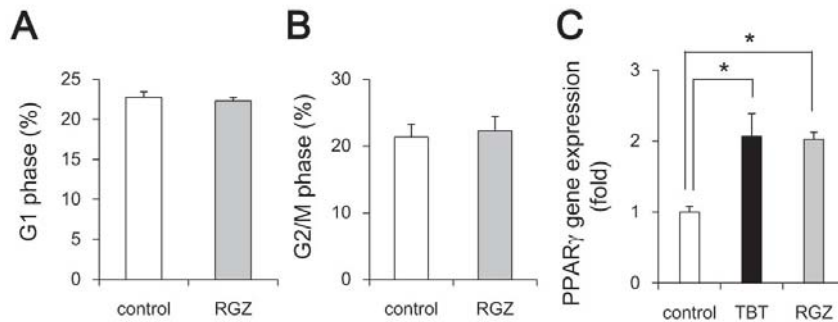


**Fig. 3.** Effect of RGZ on cell cycle progression in NT2/D1 cells. After RGZ exposure for 48 hr, cells were stained with propidium iodide (PI). The cell cycle distribution was determined by flow cytometric analysis of the DNA content using BD FACS Aria II. The ratio of G1 (A) and G2/M (B) phases was determined by Modfit LT 4.0. After exposure to TBT or RGZ, the expression of PPAR $\gamma$  was analyzed by real time PCR (C). The gene expression was comparably increased upon TBT or RGZ exposure. Data represent mean  $\pm$  S.D. (n = 3). \*P < 0.05.

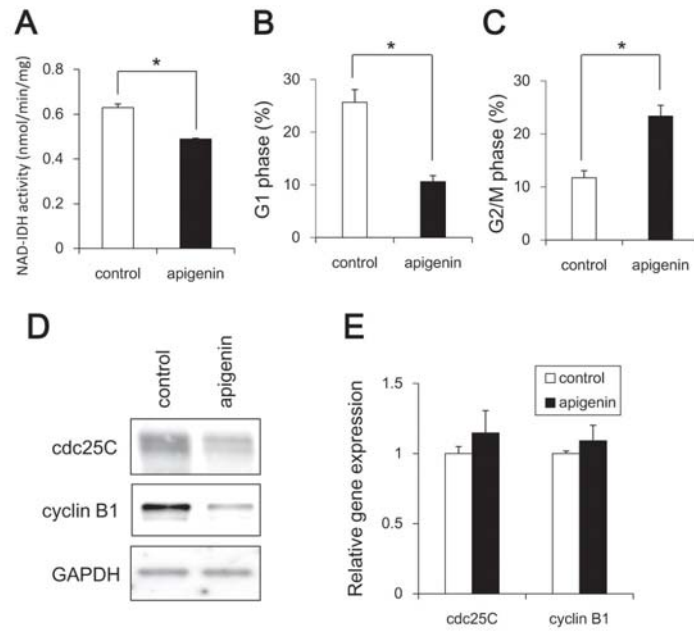


**Fig. 4.** Effect of apigenin on cell cycle progression in NT2/D1 cells. Cells were exposed to 10  $\mu$ M apigenin for 24 hr and then determined NAD-IDH activity (A). Moreover, after exposure to apigenin for 48 hr, the cell cycle distribution was determined by flow cytometric analysis of the DNA content using BD FACS Aria II. The ratio of G1 (B) and G2/M (C) phases was determined by Modfit LT 4.0. The protein expressions in the cell lysate were analyzed by western blot using anti-cdc25C, cyclin B1, or GAPDH antibodies (D). The expression of G2/M cell cycle regulators was analyzed by real time PCR (E). The gene expression was not significantly altered upon apigenin exposure. Data represent mean  $\pm$  S.D. (n = 3). \*P < 0.05.

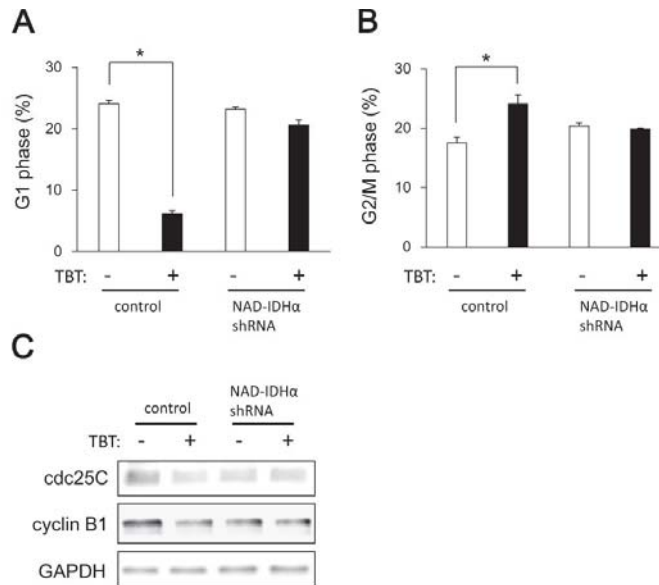


**Fig. 5.** Effect of NAD-IDH knockdown on cell cycle progression in NT2/D1 cells. Cells were infected with lentiviruses to express a shRNA against NAD-IDH $\alpha$  or a scrambled sequence shRNA (control). The infected cells were subjected to selection with 0.5  $\mu$ g/mL puromycin for 72 hr and were then exposed to TBT at 100 nM for 48 hr. After staining with PI, cell cycle distribution was determined by flow cytometric analysis of the DNA content using BD FACS Aria II. The ratio of G1 (A) and G2/M (B) phases was analyzed by Modfit LT 4.0. The protein expressions in cell lysates were analyzed by western blot using anti-cdc25C, cyclin B1, or GAPDH antibodies (C). Data represent mean  $\pm$  S.D. (n = 3). \*P < 0.05.

## TBT induces G2/M cell cycle arrest in human embryonic carcinoma

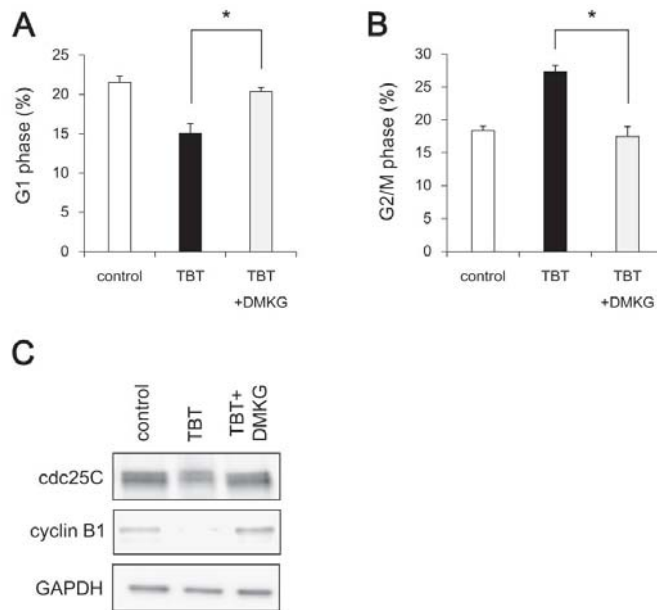


**Fig. 6.** Effect of dimethyl  $\alpha$ -ketoglutarate (DMKG) on TBT-induced G2/M cell cycle arrest in NT2/D1 cells. Cells were exposed to 100 nM TBT and 7 mM DMKG for 48 hr. Cells were then stained with propidium iodide (PI) and cell cycle distribution was determined by flow cytometric analysis of the DNA content using BD FACS Aria II. The ratio of G1 (A) and G2/M (B) phases was analyzed by Modfit LT 4.0. Next, the protein expressions in cell lysates were analyzed by western blot using anti-cdc25C, cyclin B1, or GAPDH antibodies (C). Data represent mean  $\pm$  S.D. (n = 3). \*P < 0.05.

recovered the ratio of G1 and G2/M phases to the basal level (Figs. 6A and B). DMKG treatment also recovered TBT-induced protein reduction of cdc25C and cyclin B1 (Fig. 6C). Taken together, these data suggest that NAD-IDH mediates TBT-induced G2/M cell cycle arrest via cdc25C reduction in NT2/D1 cells.

## DISCUSSION

Our data suggest that nanomolar TBT levels induce G2/M cell cycle arrest through the protein reduction of cdc25C and thereafter cyclin B1 (Figs. 1 and 2). Since the protein expression of p53 is decreased after TBT exposure, TBT-induced G2/M cell cycle arrest seems to be p53 independent. Consistent with our data, recent study has reported that nearly micromolar TBT levels induce G2/M cell cycle arrest in human amniotic cells via protein phosphatase (PP) 2A inhibition-mediated extracellular-signal-regulated kinase (ERK) inactivation (Zhang *et al.*, 2014). Since we did not observe the reduction of phospho-ERK in NT2/D1 cells after nanomolar levels of TBT exposure (data not shown), the mechanism of inducing G2 arrest may differ depending on the TBT levels and cell type. Moreover, several chemical stressors

have been reported to cause G2/M cell cycle arrest through the protein reduction of cell cycle regulators (Chaudhary *et al.*, 2013; Nam *et al.*, 2010; Ouyang *et al.*, 2009). For instance, 4-Hydroxynonenal, an inducer of oxidative stress, causes DNA damage and induces G2/M cell cycle arrest in hepatocellular carcinoma HepG2 and Hep3B cells, following reduction of cdc25C and thereafter cyclin B1 proteins in a p53-independent manner (Chaudhary *et al.*, 2013). Reduction of cdc25C protein may be mediated by the ubiquitin-proteasome system in NT2/D1 cells. Cdc25C has been reported to be degraded via ubiquitination by BRCA1 during G2/M cell cycle arrest in breast cancer cell lines (Shabbeer *et al.*, 2013). During G2/M cell cycle arrest, another cell cycle regulators, such as Plk1, cdc25A and CDK1, are also known to be degraded by ubiquitin ligases, such as multi-subunit E3 ubiquitin ligases, Skp1-Cullin1-F-box Complex (SCF) or Anaphase Promoting Complex (APC) (Bassermann and Pagano, 2010). Further studies should determine whether ubiquitin ligases are involved in TBT-induced cdc25C reduction and subsequent G2/M cell cycle arrest in embryonic cells.

Our data using apigenin showed that TBT-induced G2/M cell cycle arrest is caused by NAD-IDH inhibition

(Fig. 4) and the data were verified by NAD-IDH knockdown and DMKG experiments (Figs. 5, 6). We used apigenin as a NAD-IDH inhibitor. We also confirmed the data by knockdown experiments. Since Apigenin has been reported to inhibit not only NAD-IDH but also hnRNPA2 and NF- $\kappa$ B (Arango *et al.*, 2013), we can not rule out the possibility that apigenin-induced G2/M cell cycle arrest was induced by other targets. Our previous report indicates that TBT induces mitochondrial dysfunction, such as impaired mitochondrial morphological dynamics and reduced ATP production via NAD-IDH in embryonic carcinoma cells (Yamada *et al.*, 2015). Considering that NAD-IDH is a mitochondrial enzyme, TBT-induced G2/M cell cycle arrest is caused by mitochondrial dysfunction through NAD-IDH inhibition. NAD-IDH catalyzes the reduction of NAD to NADH, which is oxidized by the electron transport chain and is required to generate proton electrochemical gradients across the inner mitochondrial membrane (Saraste, 1999). Thus, inhibition of NAD-IDH by TBT may reduce the NADH supply, thereby dissipating the proton electrochemical gradient. Intracellular  $\text{Ca}^{2+}$  may be also involved in mitochondrial dysfunction. Previous reports have shown that several anticancer drugs induce G2/M cell cycle arrest and apoptosis by depolarizing mitochondrial membrane potential and increasing intracellular  $\text{Ca}^{2+}$  (Fang *et al.*, 2014; Guo *et al.*, 2014). With respect to intracellular  $\text{Ca}^{2+}$ , there has been also reported that TBT induces mobilization of  $\text{Ca}^{2+}$  from intracellular stores and results in phosphorylation of MAPKs because its suppression by chelation of intracellular  $\text{Ca}^{2+}$  in human T lymphoblastoid cells (Yu *et al.*, 2000). Thus,  $\text{Ca}^{2+}$  release from depolarized mitochondria may induce G2/M cell cycle arrest after TBT exposure. Further studies should determine how the downstream signaling of NAD-IDH induces reduction of the cdc25C protein and subsequent G2/M cell cycle arrest after TBT exposure in embryonic cells.

In our previous studies, we have observed that TBT degrades mitofusin proteins and induces mitochondrial fission via the NAD-IDH inhibition. Moreover, we have also shown that TBT results in growth arrest by targeting the glycolytic systems (Yamada *et al.*, 2014). Both mitochondrial fission and glycolysis have been reported to be linked to cell cycle alterations (Yamamori *et al.*, 2015; Zhai *et al.*, 2013). Thus, we are currently investigating whether TBT-induced mitochondrial fission or glycolytic inhibition are linked to G2/M cell cycle arrest or not.

In summary, we demonstrate that TBT mediates G2/M cell cycle arrest through inhibition of NAD-IDH, representing a novel non-genomic pathway of TBT-induced toxicity (Fig. 7). These negative effects of TBT on the

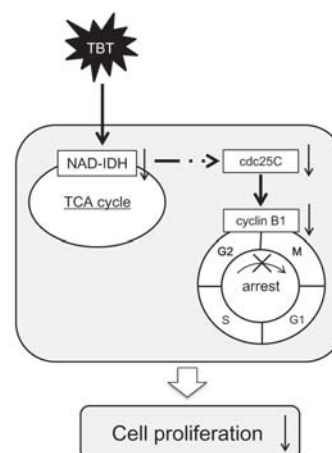


**Fig. 7.** Proposed model of TBT toxicity through non-genomic pathways in human embryonic carcinoma cells. Nanomolar TBT levels inhibit NAD-IDH activity. TBT induces G2/M cell cycle arrest via the protein reduction of cdc25C and its downstream target, cyclin B1. This TBT-induced G2/M cell cycle arrest may mediate cell growth inhibition.

cell cycle could result in direct inhibition of cell growth. Thus, TBT-induced G2/M cell cycle arrest via NAD-IDH in embryonic cells may represent a novel mechanism of cytotoxicity associated with nanomolar level exposure of EDCs.

## ACKNOWLEDGMENTS

This work was supported by a Health and Labour Sciences Research Grant from the Ministry of Health, Labour and Welfare, Japan (#H25-Kagaku-Ippan-002 to Y. Kanda), a Grant-in-Aid for Scientific Research from the Ministry of Education, Culture, Sports, Science, and Technology, Japan (#26293056, #26670041 to Y. Kanda), the Research on Regulatory Harmonization and Evaluation of Pharmaceuticals, Medical Devices, Regenerative and Cellular Therapy Products, Gene Therapy Products, and Cosmetics from Japan Agency for Medical Research and development, AMED (To Y. Sekino), and a grant from the Smoking Research Foundation (Y. Kanda).

**Conflict of interest----** The authors declare that there is no conflict of interest.

## REFERENCES

Arango, D., Morohashi, K., Yilmaz, A., Kuramochi, K., Parihar, A., Brahimaj, B., Grotewold, E. and Doseff, A.I. (2013): Molecular basis for the action of a dietary flavonoid revealed by the com-

## TBT induces G2/M cell cycle arrest in human embryonic carcinoma

- prehensive identification of apigenin human targets. *Proc. Natl. Acad. Sci. USA*, **110**, E2153-E2162.
- Bassermann, F. and Pagano, M. (2010): Dissecting the role of ubiquitylation in the DNA damage response checkpoint in G2. *Cell Death Differ.*, **17**, 78-85.
- Benkirane, K., Amiri, F., Diep, Q.N., El Mabrouk, M. and Schiffrin, E.L. (2006): PPAR-gamma inhibits ANG II-induced cell growth via SHIP2 and 4E-BP1. *Am. J. Physiol. Heart Circ. Physiol.*, **290**, H390-H397.
- Chaudhary, P., Sharma, R., Sahu, M., Vishwanatha, J.K., Awasthi, S. and Awasthi, Y.C. (2013): 4-Hydroxynonenal induces G2/M phase cell cycle arrest by activation of the ataxia telangiectasia mutated and Rad3-related protein (ATR)/checkpoint kinase 1 (Chk1) signaling pathway. *J. Biol. Chem.*, **288**, 20532-20546.
- Donzelli, M. and Draetta, G.F. (2003): Regulating mammalian checkpoints through Cdc25 inactivation. *EMBO Rep.*, **4**, 671-677.
- Dopp, E., Hartmann, L.M., Florea, A.M., Rettenmeier, A.W. and Hirner, A.V. (2004): Environmental distribution, analysis, and toxicity of organometal(loid) compounds. *Crit. Rev. Toxicol.*, **34**, 301-333.
- Fang, C., Zhang, J., Qi, D., Fan, X., Luo, J., Liu, L. and Tan, Q. (2014): Evodiamine induces G2/M arrest and apoptosis via mitochondrial and endoplasmic reticulum pathways in H446 and H1688 human small-cell lung cancer cells. *PLoS One*, **9**, e115204.
- Gabrielli, B., Brooks, K. and Pavey, S. (2012): Defective cell cycle checkpoints as targets for anti-cancer therapies. *Front. Pharmacol.*, **3**, 9.
- Gårdlund, A.T., Archer, T., Danielsen, K., Danielsson, B., Frederiksson, A., Lindquist, N.G., Lindström, H. and Luthman, J. (1991): Effects of prenatal exposure to tributyltin and trihexyltin on behaviour in rats. *Neurotoxicol. Teratol.*, **13**, 99-105.
- Guo, J., Zhao, W., Hao, W., Ren, G., Lu, J. and Chen, X. (2014): Cucurbitacin B induces DNA damage, G2/M phase arrest, and apoptosis mediated by reactive oxygen species (ROS) in leukemia K562 cells. *Anticancer Agents Med. Chem.*, **14**, 1146-1153.
- Hirata, N., Yamada, S., Shoda, T., Kurihara, M., Sekino, Y. and Kanda, Y. (2014): Sphingosine-1-phosphate promotes expansion of cancer stem cells via S1PR3 by a ligand-independent Notch activation. *Nat. Commun.*, **5**, 4806.
- Kanayama, T., Kobayashi, N., Mamiya, S., Nakanishi, T. and Nishikawa, J. (2005): Organotin compounds promote adipocyte differentiation as agonists of the peroxisome proliferator-activated receptor gamma/retinoid X receptor pathway. *Mol. Pharmacol.*, **67**, 766-774.
- Kanda, Y., Hinata, T., Kang, S.W. and Watanabe, Y. (2011): Reactive oxygen species mediate adipocyte differentiation in mesenchymal stem cells. *Life Sci.*, **89**, 250-258.
- Kawabe, T. (2004): G2 checkpoint abrogators as anticancer drugs. *Mol. Cancer Ther.*, **3**, 513-519.
- Mitra, S., Gera, R., Siddiqui, W.A. and Khandelwal, S. (2013): Tributyltin induces oxidative damage, inflammation and apoptosis via disturbance in blood-brain barrier and metal homeostasis in cerebral cortex of rat brain: an *in vivo* and *in vitro* study. *Toxicology*, **310**, 39-52.
- Nakatsu, Y., Kotake, Y., Takai, N. and Ohta, S. (2010): Involvement of autophagy via mammalian target of rapamycin (mTOR) inhibition in tributyltin-induced neuronal cell death. *J. Toxicol. Sci.*, **35**, 245-251.
- Nam, C., Doi, K. and Nakayama, H. (2010): Etoposide induces G2/M arrest and apoptosis in neural progenitor cells via DNA damage and an ATM/p53-related pathway. *Histol. Histopathol.*, **25**, 485-493.
- Ouyang, G., Yao, L., Ruan, K., Song, G., Mao, Y. and Bao, S. (2009): Genistein induces G2/M cell cycle arrest and apoptosis of human ovarian cancer cells via activation of DNA damage checkpoint pathways. *Cell Biol. Int.*, **33**, 1237-1244.
- Pani, E., Stojic, L., El-Shemerly, M., Jiricny, J. and Ferrari, S. (2007): Mismatch repair status and the response of human cells to cisplatin. *Cell Cycle*, **6**, 1796-1802.
- Saraste, M. (1999): Oxidative phosphorylation at the fin de siècle. *Science*, **283**, 1488-1493.
- Shabbeer, S., Omer, D., Berneman, D., Weitzman, O., Alpaugh, A., Pietraszkiewicz, A., Metsuyanin, S., Shainskaya, A., Papa, M.Z. and Yarden, R.I. (2013): BRCA1 targets G2/M cell cycle proteins for ubiquitination and proteasomal degradation. *Oncogene*, **32**, 5005-5016.
- Shackelford, R.E., Kaufmann, W.K. and Paules, R.S. (1999): Cell cycle control, checkpoint mechanisms, and genotoxic stress. *Environ. Health Perspect.*, **107**, 5-24.
- Whalen, M.M., Loganathan, B.G. and Kannan, K. (1999): Immunotoxicity of environmentally relevant concentrations of butyltins on human natural killer cells *in vitro*. *Environ. Res.*, **81**, 108-116.
- Willenborg, M., Panten, U. and Rustenbeck, I. (2009): Triggering and amplification of insulin secretion by dimethyl alpha-ketoglutarate, a membrane permeable alpha-ketoglutarate analogue. *Eur. J. Pharmacol.*, **607**, 41-46.
- Yamada, S., Kotake, Y., Sekino, Y. and Kanda, Y. (2013): AMP-activated protein kinase-mediated glucose transport as a novel target of tributyltin in human embryonic carcinoma cells. *Metalomics*, **5**, 484-491.
- Yamada, S., Kotake, Y., Demizu, Y., Kurihara, M., Sekino, Y. and Kanda, Y. (2014): NAD-dependent isocitrate dehydrogenase as a novel target of tributyltin in human embryonic carcinoma cells. *Sci. Rep.*, **4**, 5952.
- Yamada, S., Kotake, Y., Nakano, M., Sekino, Y. and Kanda, Y. (2015): Tributyltin induces mitochondrial fission through NAD-IDH dependent mitofusin degradation in human embryonic carcinoma cells. *Metalomics*, **7**, 1240-1246.
- Yamamori, T., Ike, S., Bo, T., Sasagawa, T., Sakai, Y., Suzuki, M., Yamamoto, K., Nagane, M., Yasui, H. and Inanami, O. (2015): Inhibition of the mitochondrial fission protein dynamin-related protein 1 (Drp1) impairs mitochondrial fission and mitoccatostrophe after X-irradiation. *Mol. Biol. Cell*, **26**, 4607-4617.
- Yu, L., Zhang, X., Yuan, J., Cao, Q., Liu, J., Zhu, P. and Shi, H. (2011): Teratogenic effects of triphenyltin on embryos of amphibian (*Xenopus tropicalis*): a phenotypic comparison with the retinoid X and retinoic acid receptor ligands. *J. Hazard Mater.*, **192**, 1860-1868.
- Yu, Z.P., Matsuoka, M., Wispriyono, B., Iryo, Y. and Igisu, H. (2000): Activation of mitogen-activated protein kinases by tributyltin in CCRF-CEM cells: role of intracellular Ca(2+). *Toxicol. Appl. Pharmacol.*, **168**, 200-207.
- Zhai, X., Yang, Y., Wan, J., Zhu, R. and Wu, Y. (2013): Inhibition of LDH-A by oxamate induces G2/M arrest, apoptosis and increases radiosensitivity in nasopharyngeal carcinoma cells. *Oncol. Rep.*, **30**, 2983-2991.
- Zhang, Y., Go, Z. and Xu, L. (2014): Tributyltin induces a G2/M cell cycle arrest in human amniotic cells via PP2A inhibition-mediated inactivation of the ERK1/2 cascades. *Environ. Toxicol. Pharmacol.*, **37**, 812-818.

# SCIENTIFIC REPORTS

OPEN

## Chlorpyrifos inhibits neural induction via Mfn1-mediated mitochondrial dysfunction in human induced pluripotent stem cells

Received: 21 October 2016  
Accepted: 13 December 2016  
Published: 23 January 2017

Shigeru Yamada<sup>1,2</sup>, Yusuke Kubo<sup>1</sup>, Daiju Yamazaki<sup>1</sup>, Yuko Sekino<sup>1</sup> & Yasunari Kanda<sup>1</sup>

Organophosphates, such as chlorpyrifos (CPF), are widely used as insecticides in agriculture. CPF is known to induce cytotoxicity, including neurodevelopmental toxicity. However, the molecular mechanisms of CPF toxicity at early fetal stage have not been fully elucidated. In this study, we examined the mechanisms of CPF-induced cytotoxicity using human induced pluripotent stem cells (iPSCs). We found that exposure to CPF at micromolar levels decreased intracellular ATP levels. As CPF suppressed energy production that is a critical function of the mitochondria, we focused on the effects of CPF on mitochondrial dynamics. CPF induced mitochondrial fragmentation via reduction of mitochondrial fusion protein mitofusin 1 (Mfn1) in iPSCs. In addition, CPF reduced the expression of several neural differentiation marker genes in iPSCs. Moreover, knockdown of *Mfn1* gene in iPSCs downregulated the expression of *PAX6*, a key transcription factor that regulates neurogenesis, suggesting that Mfn1 mediates neural induction in iPSCs. Taken together, these results suggest that CPF induces neurotoxicity via Mfn1-mediated mitochondrial fragmentation in iPSCs. Thus, mitochondrial dysfunction in iPSCs could be used as a possible marker for cytotoxic effects by chemicals.

Growing evidence suggests the involvement of environmental chemicals in neurodevelopmental toxicity, leading to neurobehavioral outcomes such as learning disabilities, attention deficit hyperactivity disorder, cognitive impairment, and autism<sup>1,2</sup>. As the fetal brain is inherently more susceptible to chemical-induced toxicity compared to the adult brain, exposure to neurotoxic chemicals during early prenatal period can cause delayed neural disorders at lower doses than in adults<sup>3,4</sup>.

Organophosphates, such as chlorpyrifos (CPF), are well known to affect brain structure and neurodevelopmental outcome, resulting in delayed neural disorders<sup>5,6</sup>. In regard to this, previous studies using magnetic resonance imaging have shown that prenatal exposure to CPF caused abnormalities in the structure, size, and thickness of cerebral cortex, where was responsible for several higher-order brain functions such as attention, cognition, and emotion<sup>7</sup>. Several reports indicate that CPF causes neurotoxicity in the developing brain of animals. In the developing brain of neonatal rats, CPF exposure impairs neurite outgrowth by inhibiting choline acetyltransferase activity<sup>8</sup>. Maternal exposure to CPF suppresses neurogenesis in the hippocampal dentate gyrus of rat offspring<sup>9</sup>. In addition to *in vivo* effects, there has been reported the cytotoxic effects of micromolar CPF levels *in vitro*. For example, CPF inhibited mitochondrial oxidative phosphorylation<sup>10</sup> and induced apoptosis in human neuroblastoma SH-SY5Y cells<sup>11</sup> or human neural precursor cells<sup>12</sup>. As micromolar CPF levels were detected in the blood of human newborns living in an agricultural community<sup>13</sup>, the observations made using micromolar levels of CPF *in vitro* could potentially reflect the biological reactions in a living body. However, the effect of CPF on neurodevelopment has not been precisely elucidated.

<sup>1</sup>Division of Pharmacology, National Institute of Health Sciences, Tokyo, Japan. <sup>2</sup>Pharmacological Evaluation Institute of Japan (PEIJ), Kanagawa, Japan. Correspondence and requests for materials should be addressed to Y.K. (email: kanda@nihs.go.jp)

Morphological changes of mitochondria are known to contribute to homeostasis<sup>14,15</sup>. Under normal circumstances, mitochondria fuses together and forms excessive tubular networks (mitochondrial fusion). These fusion is regulated by fusion factors mitofusin 1 and 2 (Mfn1, Mfn2) and optic atrophy 1 (Opa1)<sup>16,17</sup>. In contrast, under stress conditions, mitochondrial networks convert into large numbers of small fragments with spherical and punctate morphology (mitochondrial fission), and are regulated by fission factors, such as fission protein 1 (Fis1) and dynamin-related protein 1 (Drp1)<sup>18,19</sup>. This morphological dynamics contributes to the maintenance of mitochondrial functions, including energy generation<sup>14</sup>. Moreover, several studies have shown the relationship between mitochondrial fragmentation and cellular and neurodevelopmental defects. For example, Mfn1 or Mfn2 knockout mice die in midgestation embryo, accompanying with developmental delay. In addition, embryonic fibroblasts from these knockout mice display distinct types of fragmented mitochondria, a phenotype due to a severe reduction in mitochondrial fusion<sup>20</sup>. Thus, Mfn1 is considered to be functionally different from Mfn2. In support to this, Mfn1, not Mfn2, is reported to contribute to Opa1-mediated fusion of mitochondrial inner membrane<sup>16</sup>.

In the present study, we investigated the effect of CPF on neural differentiation using human induced pluripotent stem cells (iPSCs) as a model of human organ development. We focused on the effects of micromolar levels of CPF on mitochondrial dynamics, examining the molecular mechanisms of the process. Our results show that micromolar CPF levels inhibited ATP production through Mfn1 reduction, followed by mitochondrial fragmentation. Moreover, Mfn1-mediated mitochondrial dysfunction suppressed early neural induction by decreasing levels of *PAX6*, a key transcription factor that regulates neurogenesis. These data suggest that CPF-induced neurodevelopmental toxicity is based on impairment of mitochondrial functions in human iPSCs.

## Results

**Effect of CPF on neural differentiation of iPSCs.** To investigate whether CPF affects early neurodevelopment, we examined neural differentiation capability of iPSCs, which was induced by dual SMAD inhibition protocol<sup>21</sup> (Fig. 1A). First, we determined the critical CPF concentration, affecting neural differentiation. At day 4 after neural induction with different concentrations of CPF, the expression of *PAX6*, an early neuroectodermal marker that regulates neurogenesis<sup>22</sup>, was analyzed using real-time PCR. We found that exposure to 30  $\mu$ M CPF significantly decreased *PAX6* gene expression (Fig. 1B). Next, we performed time course experiments for expression of several neural differentiation markers at days 2, 4, 6, and 8 after exposure to 30  $\mu$ M CPF. At day 9, almost all cells exposed by CPF (30  $\mu$ M) were detached from the culture dish. Real-time PCR analysis revealed upregulated expression of *PAX6* by day 4, and *FOXG1*, a neuroectodermal marker that also regulates neurogenesis<sup>23</sup>, thereafter (Fig. 1C and D). Representative neural maturation marker *NCAM1*<sup>24</sup> continuously increased, confirming that further neural differentiation occurred (Fig. 1E). In addition, CPF exposure reduced the expression of these neural induction markers by day 6 (Fig. 1C–E). These data suggest that CPF has an inhibitory effect on early neural differentiation of iPSCs.

**Mitochondrial function of iPSCs exposed to CPF.** As neural differentiation process requires ATP as a source of energy<sup>25</sup>, we examined intracellular ATP content in iPSCs. Treatment with 30  $\mu$ M CPF significantly reduced the ATP content of the cells (Fig. 2A). We have previously shown that 0.1  $\mu$ M carbonyl cyanide m-chlorophenyl hydrazone (CCCP), which functions as a mitochondrial uncoupler<sup>26</sup>, decreased ATP levels in iPSCs. Because CPF inhibited ATP production, we focused on several mitochondrial functions. Mitochondrial membrane potential (MMP) was decreased by exposure to 30  $\mu$ M CPF for 24 h (Fig. 2B and C). As a positive control, exposure to 0.1  $\mu$ M CCCP reduced MMP (Figure S1). In addition, CPF exposure increased the number of cells with fragmented mitochondria displaying punctate morphology (Fig. 2D) and decreased the number of cells exhibiting mitochondrial fusion (Fig. 2E). We have already confirmed that 0.1  $\mu$ M CCCP also increased the occurrence of fragmented mitochondria. These results suggest that CPF induces mitochondrial dysfunction, including MMP depolarization and mitochondrial fragmentation, in iPSCs.

**Expression of mitochondrial fission and fusion factors in iPSCs exposed to CPF.** To examine the molecular mechanisms by which CPF induces mitochondrial fragmentation in iPSCs, we assessed the expression levels of mitochondrial fission (*Fis1* and *Drp1*) and fusion genes (*Mfn1*, *Mfn2*, and *OPA1*). Real-time PCR analysis showed that the gene expression of the factors was not altered after CPF exposure (Fig. 3A). Interestingly, western blot analysis revealed that CPF significantly decreased Mfn1 protein levels. In contrast, protein expression levels of other factors, including Mfn2, were not changed (Fig. 3B and C). These data suggest that CPF-induced mitochondrial fragmentation is caused by reduction of Mfn1 protein levels.

**Effects of CPF in iPSC-derived neural progenitor cells.** To investigate whether the effects of CPF selectively occur in the early stage of neural differentiation in iPSCs, we used iPSC-derived neural progenitor cells (NPCs), which were induced by dual SMAD inhibition protocol<sup>21</sup> (Figure S1A). Treatment with 30  $\mu$ M CPF had little effect on ATP content (Figure S1B). Similarly, exposure to 30  $\mu$ M CPF had little effect on mitochondrial morphology (Figure S1C and D), which was confirmed by the fact that CPF did not alter the protein levels of mitochondrial fission and fusion factors containing Mfn1 (Figure S1E). These data suggest that iPSCs, not NPCs, are sensitive to CPF exposure.

**Effect of Mfn1 knockdown on neural induction of iPSCs.** To further investigate the involvement of Mfn1 in the effects of CPF on neural induction, we performed knockdown (KD) of Mfn1, using lentivirus-delivered shRNAs. Real-time PCR analysis showed that KD was selective for *Mfn1*, not *Mfn2*, and that the efficiency was approximately 70% (Fig. 4A). The KD effects were also confirmed by protein levels (Fig. 4B and C). The Mfn1 KD cells were used to perform neural induction. Real-time PCR analysis revealed that Mfn1 KD

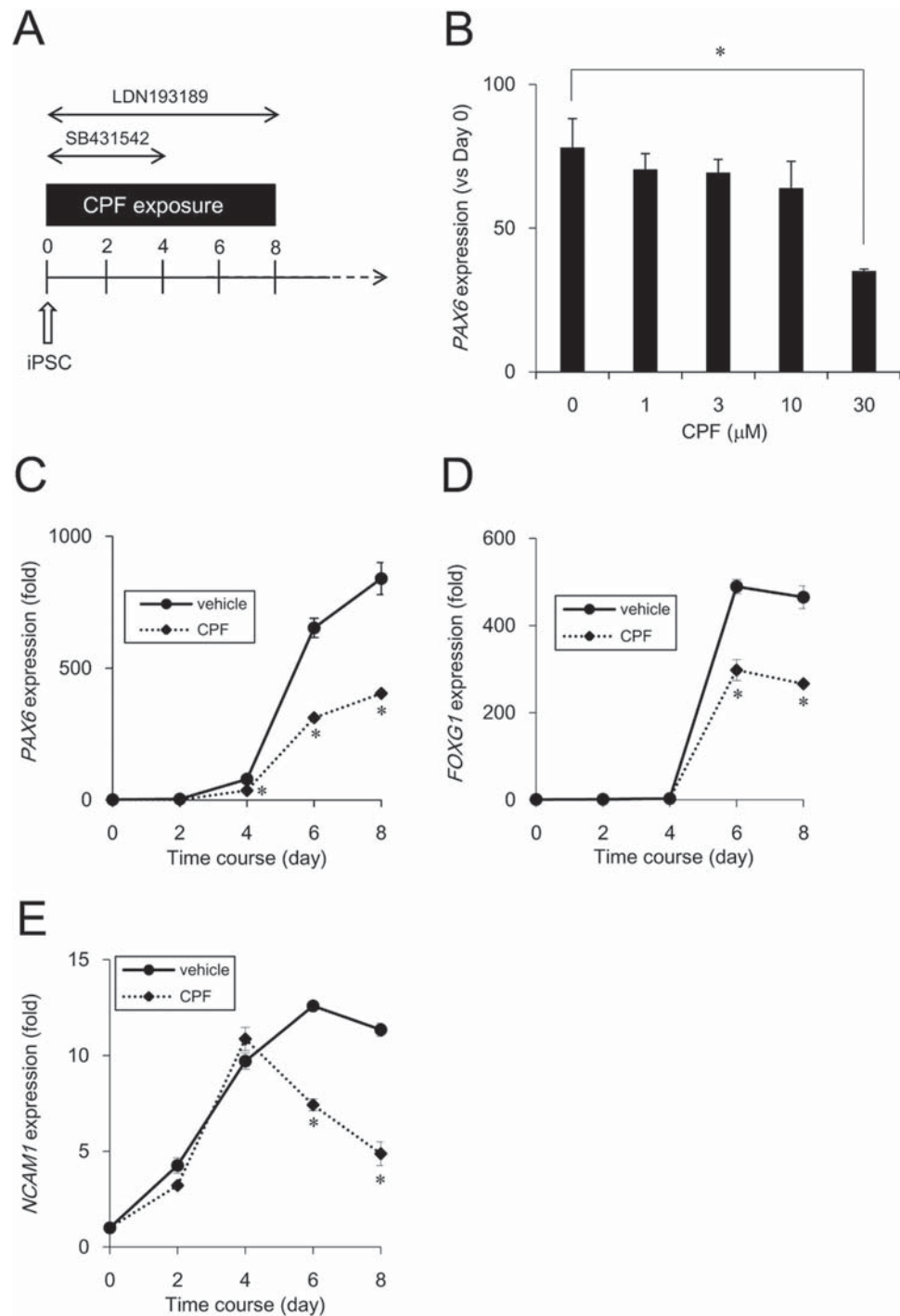


**Figure 1. Time course studies of neural induction in iPSCs exposed to CPF.** (A) Schematic time course of induction from iPSCs to NPCs by dual SMAD inhibition. Neural induction was initiated after exposure to CPF for 24 h. The cells were continuously exposed to CPF throughout neural differentiation. (B) At day 4 after neural induction with CPF (0–30  $\mu\text{M}$ ), expression of the neural differentiation marker *PAX6* was examined using real-time PCR analysis. (C–E) At days 2, 4, 6, and 8 after neural induction with CPF (30  $\mu\text{M}$ ), expression of neural differentiation markers, *PAX6*, *FOXG1*, and *NCAM1* was examined using real-time PCR analysis. Data are represented as means  $\pm$  SD ( $n = 3$ ). \* $P < 0.05$ .

decreased the expression of *PAX6* (day 4), *FOXG1* (day 6) and *NCAM1* (day 6) (Fig. 4D). These data suggest that Mfn1 is involved in CPF-mediated negative effects on neural induction of iPSCs.

**Negative regulation of neural induction by CPF exposure.** A previous report indicates that ERK signaling inhibits neural induction via *PAX6* silencing in human embryonic stem cells<sup>27</sup>. ERK has been reported to be activated after depletion of Mfn1<sup>28</sup>. We focused on ERK signaling in the effect of CPF on neural induction.

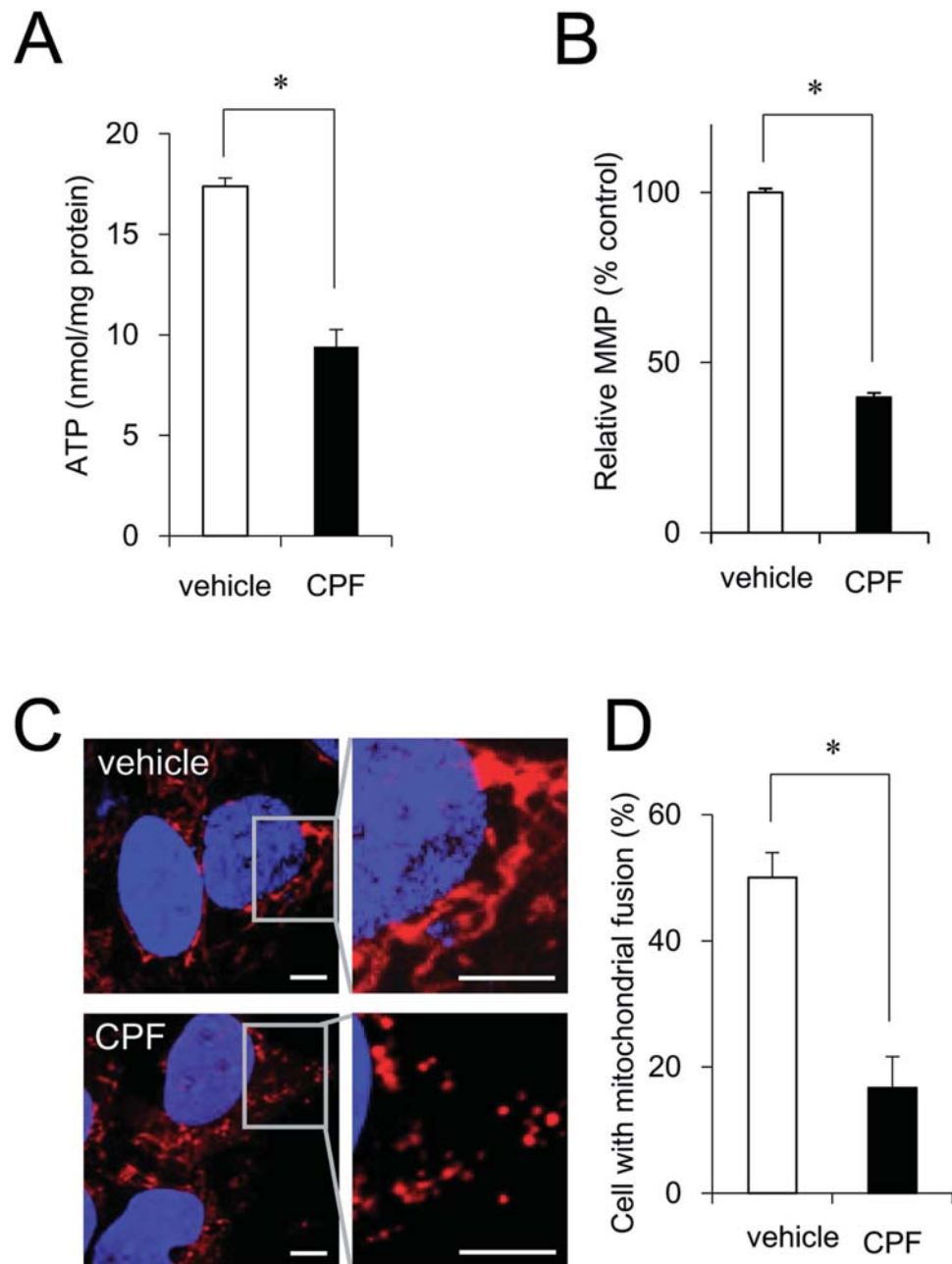


**Figure 2. Mitochondrial function of iPSCs exposed to CPF.** (A) Cells were exposed to CPF (30  $\mu$ M) for 24 h. Intracellular ATP content was determined in the lysed cells (n = 3). (B) Cells were exposed to CPF for 24 h and stained with JC-10 for 20 min. MMP of JC-10 labeled cells was analyzed by flow cytometry. The histogram represents the ratio of JC-aggregate (F-590) to JC-monomer (F-535) fluorescence (n = 3). (C) Cells were exposed to CPF for 72 h and stained with MitoTracker Red CMXRos and Hoechst33342. Mitochondrial morphology was observed by confocal laser microscopy. Bar = 5  $\mu$ m. (D) The number of cells with mitochondrial fusion (<10% punctiform) was determined in each image (n = 5). Data are represented as means  $\pm$  SD. \* $P$  < 0.05.

We found that CPF exposure significantly increased basal ERK phosphorylation levels, which were abolished by treatment with the ERK inhibitor U0126 (Fig. 5A and B). To further study whether *PAX6* downregulation in CPF-exposed cells occurred through ERK signaling, we examined the effect of U0126 on *PAX6* expression. Incubation with U0126 recovered the expression levels of *PAX6* (Fig. 5C). These data suggest that CPF activates ERK and prevents neural induction via *PAX6* downregulation.

**Effect of Mfn1 knockdown on neural induction.** To confirm the involvement of Mfn1 in the inhibition of neural induction by CPF, we used Mfn1 KD cells. Mfn1 KD significantly increased basal ERK phosphorylation levels that were abolished by treatment with the ERK inhibitor U0126 (Fig. 6A and B). To further study

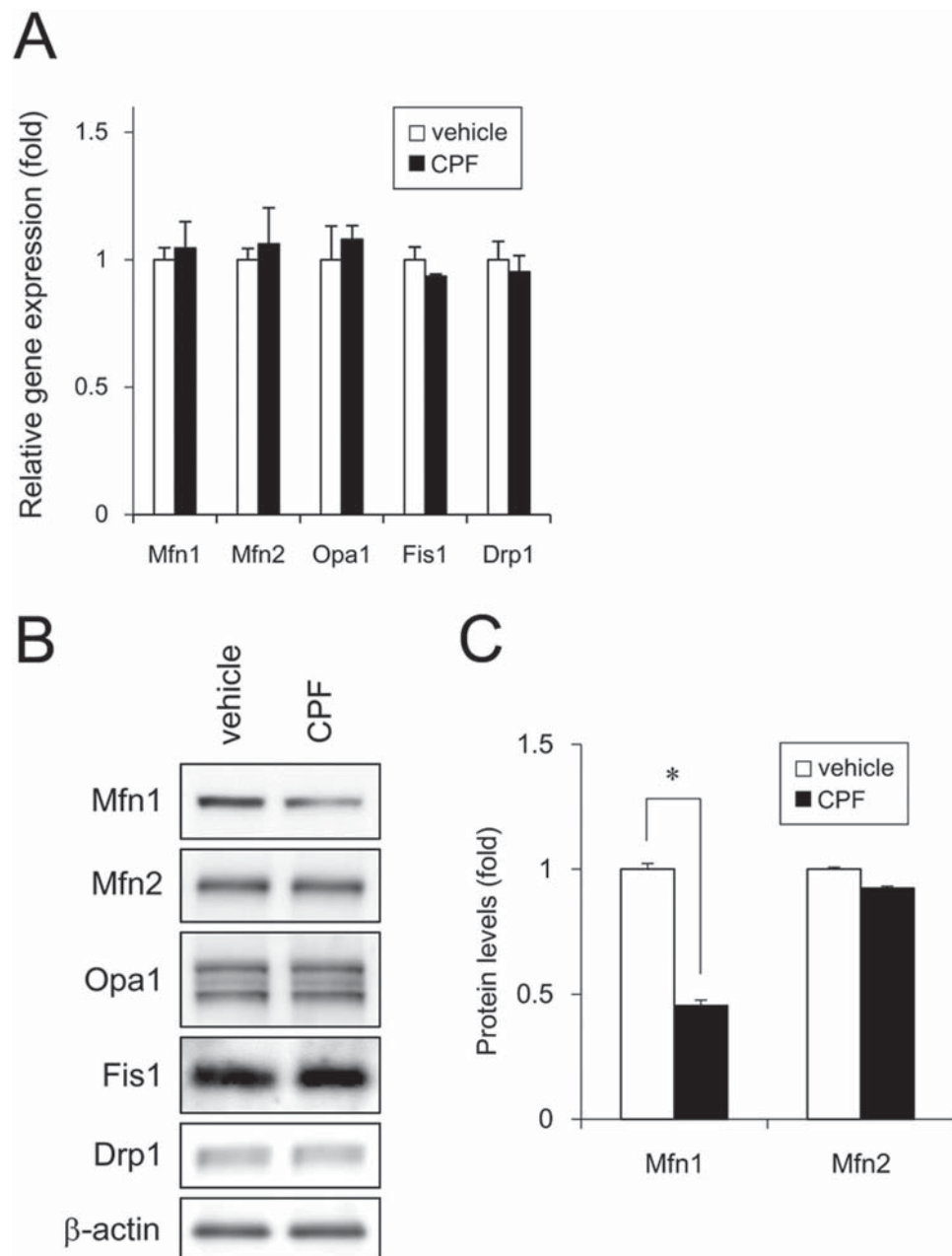


**Figure 3. Expression of mitochondrial fission and fusion factors of iPSCs exposed to CPF.** (A) After exposure to CPF (30  $\mu$ M) for 24 h, expression of mitochondrial genes was analyzed by real-time PCR. (B) After exposure to CPF for 24 h, expression of mitochondrial proteins was analyzed by western blotting using anti-Drp1, anti-Fis1, anti-Mfn1, anti-Mfn2, anti-Opa1, or anti- $\beta$ -actin antibodies. (C) Relative densities of bands were quantified with ImageJ software. Relative changes in expression were determined by normalization to  $\beta$ -actin. Data are represented as means  $\pm$  SD (n = 3). \* $P < 0.05$ .

whether *PAX6* downregulation in Mfn1 KD cells occurred through ERK signaling, we examined the effect of U0126 on *PAX6* expression. Mfn1 KD decreased *PAX6* by 64% by in the vehicle-treated cells. In contrast, Mfn1 KD decreased *PAX6* by 30% in the U0126-treated cells. Thus, incubation with U0126 partially recovered the *PAX6* expression in the Mfn1 KD cells (Fig. 6C). Taken together, these data suggest that Mfn1 reduction by CPF exposure activates ERK and prevents neural induction via *PAX6* downregulation.

### Discussion

In the present study, we demonstrated that exposure to micromolar CPF targeted mitochondrial quality control in human iPSCs. We showed that CPF induced Mfn1 reduction, thereby promoting mitochondrial fragmentation. These negative effects of CPF on mitochondrial quality control could suppress ATP production and neural

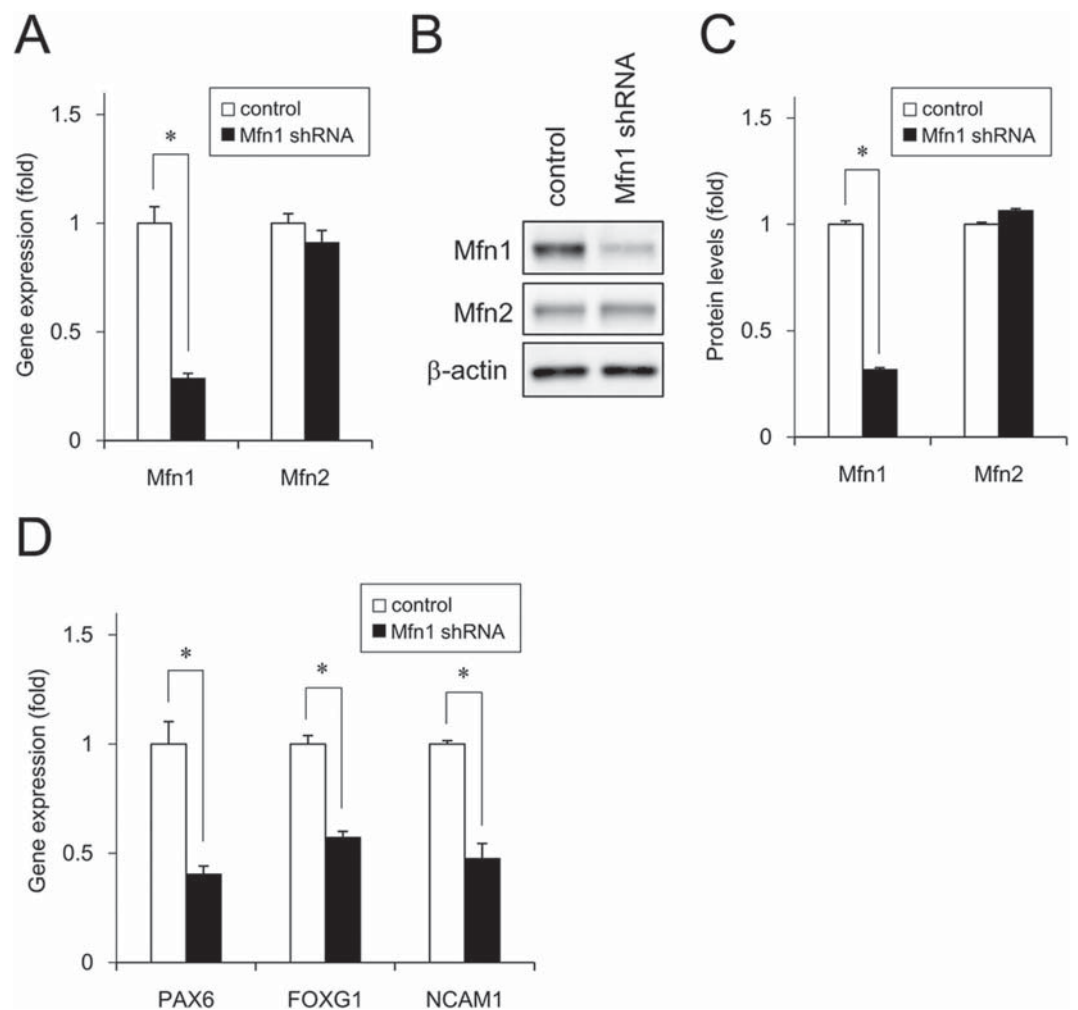


**Figure 4. Effect of Mfn1 knockdown on neural induction of iPSCs.** Cells were infected with lentiviruses containing a vector encoding a shRNA directed against *Mfn1* or a scrambled sequence shRNA (control) for 24 h. The infected cells were subjected to selection with puromycin (1  $\mu$ g/ml) for 24 h and cultured for an additional 72 h prior to functional analyses. **(A)** The expression of *Mfn1* and *Mfn2* genes was analyzed by real-time PCR. **(B)** The expression of Mfn1 and Mfn2 proteins was analyzed by western blotting using anti-Mfn1, anti-Mfn2, or anti- $\beta$ -actin antibodies. **(C)** Relative densities of bands were quantified with ImageJ software. Relative changes in expression were determined by normalization to  $\beta$ -actin. **(D)** Expression of neural differentiation markers *PAX6* (day 4), *FOXG1* (day 6), and *NCAM1* (day 6) was examined with real-time PCR. Data are represented as means  $\pm$  SD (n = 3). \* $P$  < 0.05.

differentiation. Based on the data observed in our study, Fig. 7 shows a proposed mechanism of CPF cytotoxicity via mitochondrial dysfunction.

Our studies showed that treatment with micromolar CPF levels caused mitochondrial dysfunction of human iPSCs (Fig. 2). We observed that iPSCs were sensitive to CPF exposure, unlike iPSC-derived NPCs (Figure S1). Previous reports support this difference in CPF sensitivity. The inhibitory effect of CPF on DNA synthesis in undifferentiated C6 glioma cells is found to be much higher than in differentiated cells<sup>29</sup>. *In vivo* studies indicate that immature organisms are more susceptible to CPF-induced toxicity compared to adults due to lower levels of CPF metabolizing enzymes<sup>30</sup>. Thus, the difference in CPF sensitivity between iPSCs and NPCs may be dependent on the maturation of CPF detoxification pathways. We are currently conducting experiments to determine the mechanism causing the differences in sensitivity to CPF.

We showed that CPF induced mitochondrial fragmentation via Mfn1 reduction (Figs 2 and 3). Consistent with this, our previous knockdown studies indicated that Mfn1 reduction was sufficient to promote mitochondrial dysfunction<sup>31</sup>. CPF-induced Mfn1 reduction might mediate mitochondrial fragmentation, decrease ATP levels, and inhibit iPSC growth. Although Mfn2 is also involved in mitochondrial fission and energy supply processes<sup>32,33</sup>, our results indicated that CPF specifically targeted Mfn1, not Mfn2. Regarding this apparent CPF specificity, E3 ubiquitin ligase membrane-associated RING-CH 5 (MARCH5) has been reported to selectively bind to Mfn1 dependent on its acetylation, and degrade among all mitochondrial proteins, including Mfn2<sup>34</sup>. In addition, we have reported that organotin compounds induced Mfn1 degradation through MARCH5,

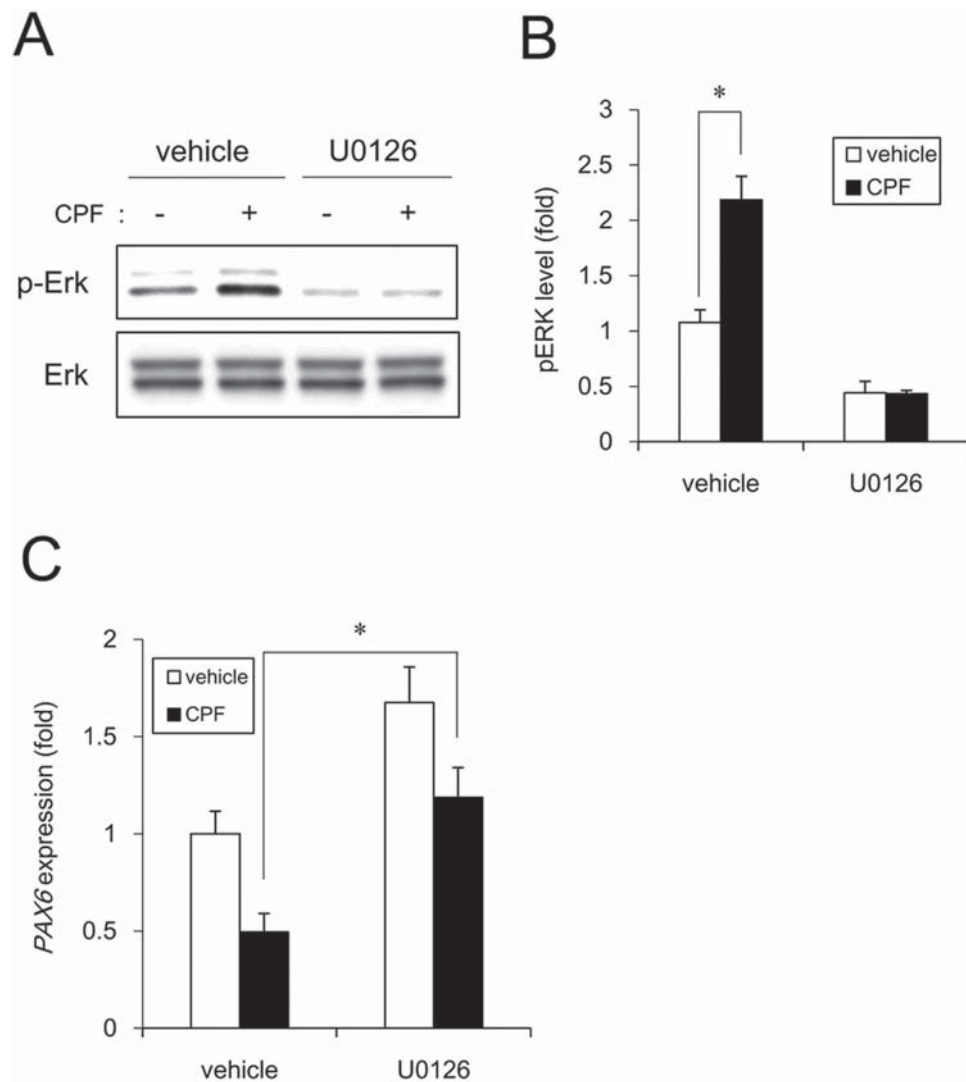


**Figure 5. Negative regulation of neural induction by CPF exposure.** (A) Cells were exposed to CPF (30  $\mu$ M) or CPF + U0126 (5  $\mu$ M) for 24 h. ERK phosphorylation was analyzed by western blotting using anti-phospho-ERK antibodies. (B) Relative densities of bands changes were quantified with ImageJ software. Relative changes in expression were determined by normalization to total ERK protein level. (C) At day 4 after neural induction with CPF or CPF + U0126, the expression of *PAX6* gene was analyzed by real-time PCR. Data are represented as means  $\pm$  SD (n = 3). \* $P < 0.05$ .

thereby promoting mitochondrial fragmentation in iPSCs<sup>31</sup>. Thus, CPF may specifically target Mfn1 protein via MARCH5 in iPSCs without affecting mRNA levels. Furthermore, the difference in CPF sensitivity between iPSCs and NPCs may be dependent on Mfn1 and MARCH5 expression levels or MARCH5 activity. Further studies should determine whether CPF reduces Mfn1 via MARCH5-mediated degradation in iPSCs.

We demonstrated that ERK phosphorylation mediated the negative effects of CPF on early neural differentiation (Figs 1, 4 and 5). A previous report indicates that Mfn1 directly binds Ras and Raf, resulting in the inhibition of Ras-Raf-ERK signaling by the biochemical analysis<sup>35,36</sup>. Mfn1 reduction by CPF or shRNA may reverse this ERK signaling inhibition. Mobilization of  $Ca^{2+}$  from intracellular stores, including mitochondria was reported to result in phosphorylation of MAPKs, as the process was suppressed by chelation of intracellular  $Ca^{2+}$  in human T lymphoblastoid cells<sup>37</sup>. As mitochondria are known to uptake into the matrix of any  $Ca^{2+}$  that has accumulated in the cytosol, dependent on MMP<sup>38</sup>, mitochondrial dysfunction by CPF exposure may cause an overload of  $Ca^{2+}$ , resulting in ERK activation. Moreover, ERK signaling was reported to inhibit neural induction by *PAX6* silencing via upregulation of stemness factors *NANOG/OCT4* and downregulation of homeobox transcription factor *OTX2*<sup>27</sup>. *NANOG* and *OCT4* act as repressors of *PAX6* induction, whereas *OTX2* is a positive inducer of *PAX6*<sup>27</sup>. Therefore, ERK signaling evoked by CPF could affect the expression of these transcriptional network, including *NANOG*, *OCT4* and *OTX2*, by regulating *PAX6*. In future studies, we should further investigate the mechanisms of CPF-induced negative regulation of neural induction via ERK.

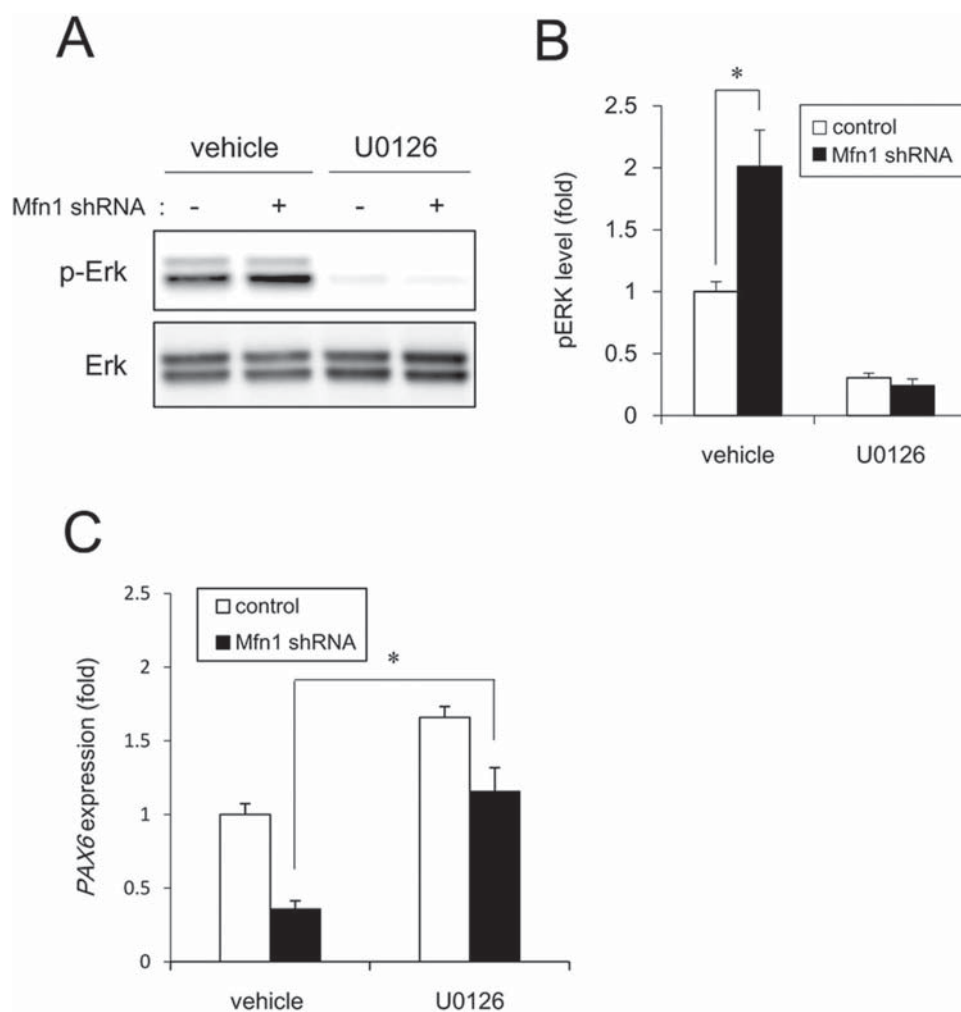


**Figure 6. Negative regulation of neural induction by Mfn1 knockdown.** The cells were infected with lentiviruses containing a vector encoding a shRNA directed against Mfn1 or a scrambled sequence shRNA (control) for 24 h. The infected cells were subjected to selection with 1  $\mu$ g/ml puromycin for 24 h and cultured for an additional 72 h prior to functional analyses. **(A)** After incubation with U0126 for 24 h, ERK phosphorylation was analyzed by western blotting using anti-phospho-ERK antibodies. **(B)** Relative densities of bands were quantified with ImageJ software. Relative changes in expression were determined by normalization to total ERK protein level. **(C)** At day 4 after neural induction with U0126, the expression of *PAX6* gene was analyzed by real-time PCR. Data are represented as means  $\pm$  SD (n = 3). \**P* < 0.05.

We further demonstrated that Mfn1 reduction mediated cytotoxic effects of CPF on iPSCs via *PAX6* down-regulation (Figs 5 and 6). *FOXG1* was downregulated, along with *PAX6*, during neural differentiation of iPSCs exposed to CPF. *PAX6* and *FOXG1* act as transcriptional regulators during forebrain development in vertebrates<sup>39,40</sup>. Targeted disruption of *PAX6* and *FOXG1* in rodents led to the loss of anterior neural tissues, suggesting the central role of these genes in forebrain development<sup>41,42</sup>. CPF causes various defects in the development of hippocampus and cortex of rodents<sup>43</sup>. Thus, CPF-induced defects of forebrain architecture may be caused by transcriptional silencing of anterior neural markers during early neurogenesis. As *NCAM1* was downregulated during neural differentiation of iPSCs exposed to CPF, further studies using NPCs are required to reveal how CPF affects neural maturation processes.

In summary, our results demonstrate a novel mechanism underlying cytotoxicity, including neurodevelopmental toxicity of CPF in iPSCs. Recently, significant progress has been made in the induction of differentiation of pluripotent stem cells into a variety of cell types<sup>44</sup>. Further studies are needed to evaluate the developmental effects of CPF on various types of iPSC-derived cells. Moreover, we show that CPF toxicity is caused by Mfn1-mediated mitochondrial dysfunction, which is involved in the cytotoxicity of organotin compounds<sup>31</sup>. Thus, mitochondrial functions influenced by Mfn1 might be a good starting point for investigating toxic mechanisms induced by exposure to other chemicals.

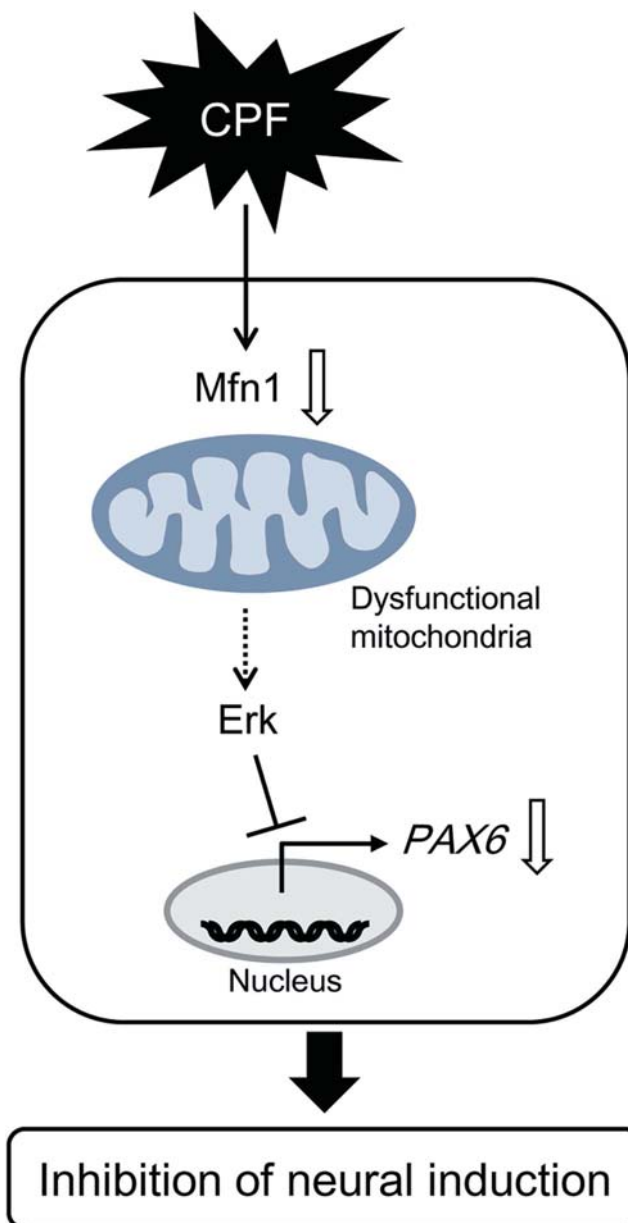


**Figure 7. Proposed mechanism of CPF cytotoxicity in human iPSCs.** CPF exposure causes Mfn1 reduction, which induces mitochondrial dysfunction, including mitochondrial fragmentation and decreased ATP levels. Mitochondrial dysfunction in turn evokes ERK phosphorylation, leading to the suppression of *PAX6*, which is an early marker of neurogenesis.

## Methods

**Chemicals.** Chlorpyrifos (CPF), Y-27632, SB431542, and LDN193189 were obtained from Wako (Tokyo, Japan). Penicillin-streptomycin mixture (PS) was obtained from Thermo Fisher Scientific (Waltham, MA, USA). U0126 was obtained from Enzo Life Sciences (Farmingdale, NY, USA). Poly-L-ornithine, 2-mercaptoethanol (2-ME), and carbonylcyanide *m*-chlorophenylhydrazine (CCCP) were obtained from Sigma-Aldrich (St. Louis, MO, USA). All other reagents were of analytical grade and obtained from commercial sources.

**Cell culture.** Human iPSC line 253G1 (Riken BRC Cell Bank, Tsukuba, Ibaraki, Japan) was established through retroviral transduction of *OCT4*, *SOX2*, and *KLF4* into adult human dermal fibroblasts<sup>45</sup>. The cells were cultured under feeder-free conditions using human embryonic stem cell (ESC)-qualified Matrigel (BD Biosciences, San Jose, CA, USA) and TeSR-E8 medium (Stemcell Technologies, Vancouver, BC, Canada) at 37 °C in an atmosphere containing 5% CO<sub>2</sub>. For passage, iPSC colonies were dissociated into single cells using Accumax (Innovative Cell Technologies, San Diego, CA, USA) and cultured in TeSR-E8 medium supplemented with Y-27632 (ROCK inhibitor, 10 μM). The NPCs derived from iPSCs were cultured on poly-L-ornithine and Laminin (Thermo Fisher Scientific) coated dishes at 37 °C in an atmosphere containing 5% CO<sub>2</sub>. The culture

medium was Neural maintenance medium [NMM; a 1 : 1 mixture of DMEM/F12 (Thermo Fisher Scientific) and Neurobasal (Thermo Fisher Scientific) containing N2 (Thermo Fisher Scientific), B27 (Thermo Fisher Scientific), GlutaMAX (Thermo Fisher Scientific), non-essential amino acids (NEAA; Thermo Fisher Scientific), 2-ME, PS]. For passage, NPCs were dissociated into single cells using Accumax and cultured in NMM supplemented with EGF (20 ng/ml), FGF2 (20 ng/ml) and Y-27632.

**Neural differentiation procedure.** For the induction of neuronal lineages, dual SMAD inhibition protocol was used as previously described<sup>21</sup> with modifications. Briefly, iPSC colonies were dissociated into single cells with Accumax. The cells were seeded at a density of  $7 \times 10^4$  cells/cm<sup>2</sup> in TeSR-E8 medium on Matrigel-coated plates in order to reach nearly confluent within two days after seeding. The initial differentiation medium was knockout serum replacement (KSR) medium [Knockout DMEM (Thermo Fisher Scientific) containing KSR (Thermo Fisher Scientific), L-glutamine, NEAA, 2-ME, PS] with SB431542 (TGF $\beta$  inhibitor, 10  $\mu$ M) and LDN193189 (BMP inhibitor, 1  $\mu$ g/ml). After 4 days, N2 medium [Neurobasal containing N2, B27, GlutaMAX, PS] was added to the KSR medium with LDN193189 every two days.

**Measurement of intracellular ATP levels.** Intracellular ATP content was measured using an ATP Determination Kit (Thermo Fisher Scientific), according to the manufacturer's protocol. Briefly, the cells were washed and lysed with 0.1% Triton X-100/PBS. The resulting cell lysates were added to a reaction mixture containing 0.5 mM D-luciferin, 1 mM DTT, and 1.25  $\mu$ g/mL luciferase and incubated for 30 min at room temperature. Luminescence was measured using a Fluoroskan Ascent FL microplate reader (Thermo Fisher Scientific). The luminescence intensities were normalized to the total protein content.

**Measurement of MMP.** A Cell Meter JC-10 Mitochondrial Membrane Potential Assay Kit (AAT Bioquest, Sunnyvale, CA, USA) was used to detect MMP. Briefly, the cells were suspended in staining buffer containing JC-10 and incubated for 20 min at room temperature. After the cells were treated with CPF, a FACS Aria II cell sorter (BD Biosciences) was used to measure the fluorescence intensity ratio, JC-aggregate (F-590)/JC-monomer (F-535).

**Assessment of mitochondrial fusion.** After treatment with CPF (30  $\mu$ M, 72 h), the cells were fixed with 4% paraformaldehyde and stained with 50 nM MitoTracker Red CMXRos (Cell Signaling Technology, Danvers, MA, USA) and 5  $\mu$ g/mL Hoechst 33342 (Sigma-Aldrich). Changes in mitochondrial morphology were observed using a confocal laser microscope (Nikon A1). Images ( $n = 5$ ) of random fields were taken, and the number of cells displaying mitochondrial fusion (<10% punctiform) was determined in each image, as previously reported<sup>46</sup>.

**Real-time polymerase chain reaction (PCR).** Total RNA was isolated from iPSCs using TRIzol reagent (Thermo Fisher Scientific), and quantitative real-time reverse transcription (RT)-PCR was performed using a QuantiTect SYBR Green RT-PCR Kit (Qiagen, Valencia, CA, USA) on an ABI PRISM 7900HT sequence detection system (Applied Biosystems, Foster City, CA, USA) as previously reported<sup>47</sup>. Relative changes in transcript levels were normalized to the mRNA levels of glyceraldehyde-3-phosphate dehydrogenase (*GAPDH*). The following primer sequences were used for real-time PCR analysis: *Fis1*, forward, 5'-TACGTCCGCGGGTTGCT-3' and reverse, 5'-CCAGTTCCTTGGCCTGGTT-3'; *Drp1*, forward, 5'-TGGGCGCCGACATCA-3' and reverse, 5'-GCTCTGCGTTCCTACTACGA-3'; *Mfn1*, forward, 5'-GGCATCTGTGGCCGAGTT-3' and reverse, 5'-ATTATGCTAAGTCTCCGCTCCAA-3'; *Mfn2*, forward, 5'-GCTCGGAGGCACATGAAAGT-3' and reverse, 5'-ATCACGGTGCTCTTCCCATT-3'; *Opa1*, forward, 5'-GTGCTGCCCGCCTAGAAA-3' and reverse, 5'-TGACAGGCACCCGTAAGT-3'; *PAX6*, forward, 5'-ATGTGTGAGTAAAATTCTGGGCA-3' and reverse, 5'-GCTTACAACCTTCTGGAGTCGCTA-3'; *FOXG1*, forward, 5'-GCCACAATCTGTCCCTCAACA-3' and reverse, 5'-GACGGGTCCAGCATCCAGTA-3'; *NCAM1*, forward, 5'-GGCATTTACAAGTGTGTGGTTAC-3' and reverse, 5'-TTGGCGCATTCTTGAACATGA-3'; *GAPDH*, forward, 5'-GTCTCCTCTGACTTCAACAGCG-3' and reverse, 5'-ACCACCCTGTTGCTGTAGCCAA-3'.

**Western blot analysis.** Western blot analysis was performed as previously reported<sup>48</sup>. Briefly, the cells were lysed with Cell Lysis Buffer (Cell Signaling Technology). The proteins were then separated by sodium dodecyl sulfate-polyacrylamide gel electrophoresis (SDS-PAGE) and electrophoretically transferred to Immobilon-P membranes (Millipore, Billerica, MA, USA). The membranes were probed with anti-Drp1 monoclonal antibodies (1:1000; Cell Signaling Technology), anti-Fis1 polyclonal antibodies (1:200; Santa Cruz Biotechnology, Santa Cruz, CA, USA), anti-Mfn1 polyclonal antibodies (1:1000; Cell Signaling Technology), anti-Mfn2 monoclonal antibodies (1:1000; Cell Signaling Technology), anti-Opa1 monoclonal antibodies (1:1000; BD Biosciences), anti-ERK1/2 polyclonal antibodies (1:1000; Cell Signaling Technology), anti-phospho ERK1/2 (Thr202/Tyr204) monoclonal antibodies (1:2000; BD Biosciences), and anti- $\beta$ -actin monoclonal antibodies (1:5000; Sigma-Aldrich). The membranes were then incubated with secondary antibodies against rabbit or mouse IgG conjugated to horseradish peroxidase (Cell Signaling Technology). The bands were visualized using an ECL Western Blotting Analysis System (GE Healthcare, Buckinghamshire, UK). Images were acquired using an LAS-3000 Imager (FUJIFILM, Tokyo, Japan).

**Gene knockdown by shRNA.** Knockdown experiments were performed using *Mfn1* shRNA lentiviruses from Sigma-Aldrich (MISSION shRNA), as previously reported<sup>49</sup>. A scrambled hairpin sequence was used as a

negative control. Briefly, the cells were infected with the viruses at a multiplicity of infection of 1 in the presence

of 8 µg/mL hexadimethrine bromide (Sigma-Aldrich) for 24 h. After medium exchange, the cells were subjected to selection with 1 µg/mL puromycin for 24 h and cultured for an additional 72 h prior to functional analyses.

**Statistical analysis.** All data are presented as means ± standard deviation (SD). Analysis of variance (ANOVA) followed by post-hoc Bonferroni test was used to analyze data in Figs 1, 3C, 4, 5, and 6. Student's t test was used to analyze data in Figs 2, 3A, S1, and S2. *P*-values < 0.05 were considered statistically significant.

## References

- Landrigan, P. J., Lambertini, L. & Birnbaum, L. S. A research strategy to discover the environmental causes of autism and neurodevelopmental disabilities. *Environ. Health Perspect.* **120**, a258–a260 (2012).
- Ross, E. J., Graham, D. L., Money, K. M. & Stanwood, G. D. Developmental consequences of fetal exposure to drugs: what we know and what we still must learn. *Neuropsychopharmacology* **40**, 61–87 (2015).
- Rodier, P. M. Developing brain as a target of toxicity. *Environ. Health Perspect.* **103**, 73–76 (1995).
- Rice, D. & Barone, S. Jr. Critical periods of vulnerability for the developing nervous system: evidence from humans and animal models. *Environ. Health Perspect.* **108**, 511–533 (2000).
- Brown, M. A. & Brix, K. A. Review of health consequences from high-, intermediate- and low-level exposure to organophosphorus nerve agents. *J. Appl. Toxicol.* **18**, 393–408 (1998).
- Ray, D. E. & Richards, P. G. The potential for toxic effects of chronic, low-dose exposure to organophosphates. *Toxicol. Lett.* **120**, 343–351 (2001).
- Rauh, V. A. *et al.* Brain anomalies in children exposed prenatally to a common organophosphate pesticide. *Proc. Natl. Acad. Sci. USA* **109**, 7871–7876 (2012).
- Slotkin, T. A., Levin, E. D. & Seidler, F. J. Comparative developmental neurotoxicity of organophosphate insecticides: effects on brain development are separable from systemic toxicity. *Environ. Health Perspect.* **114**, 746–751 (2006).
- Ohishi, T. *et al.* Reversible effect of maternal exposure to chlorpyrifos on the intermediate granule cell progenitors in the hippocampal dentate gyrus of rat offspring. *Reprod. Toxicol.* **35**, 125–136 (2013).
- Salama, M., El-Morsy, D., El-Gamal, M., Shabka, O. & Mohamed, W. M. Mitochondrial complex I inhibition as a possible mechanism of chlorpyrifos induced neurotoxicity. *Ann. Neurosci.* **21**, 85–89 (2014).
- Lee, J. E., Park, J. H., Jang, S. J. & Koh, H. C. Rosiglitazone inhibits chlorpyrifos-induced apoptosis via modulation of the oxidative stress and inflammatory response in SH-SY5Y cells. *Toxicol. Appl. Pharmacol.* **278**, 159–171 (2014).
- Lee, J. E., Lim, M. S., Park, J. H., Park, C. H. & Koh, H. C. Nuclear NF-κB contributes to chlorpyrifos-induced apoptosis through p53 signaling in human neural precursor cells. *Neurotoxicology* **42**, 58–70 (2014).
- Huen, K. *et al.* Organophosphate pesticide levels in blood and urine of women and newborns living in an agricultural community. *Environ. Res.* **117**, 8–16 (2012).
- Youle, R. J. & van der Bliek, A. M. Mitochondrial fission, fusion, and stress. *Science* **337**, 1062–1065 (2012).
- van der Bliek, A. M., Shen, Q. & Kawajiri, S. Mechanisms of mitochondrial fission and fusion. *Cold Spring Harb. Perspect. Biol.* **5**, pii: a011072 (2013).
- Cipolat, S., De Brito, O. M., Dal Zilio, B. & Scorrano, L. OPA1 requires mitofusin 1 to promote mitochondrial fusion. *Proc. Natl. Acad. Sci. USA* **101**, 15927–15932 (2004).
- Koshiba, T. *et al.* Structural basis of mitochondrial tethering by mitofusin complexes. *Science* **305**, 858–862 (2004).
- Smirnova, E., Griparic, L., Shurland, D.-L. & van der Bliek, A. M. Dynamin-related protein Drp1 is required for mitochondrial division in mammalian cells. *Mol. Biol. Cell* **12**, 2245–2256 (2001).
- Yoon, K., Krueger, E. W., Oswald, B. J. & McNiven, M. A. The mitochondrial protein hFis1 regulates mitochondrial fission in mammalian cells through an interaction with the dynamin-like protein DLP1. *Mol. Biol. Cell* **23**, 5409–5420 (2003).
- Chen, H. *et al.* Mitofusins Mfn1 and Mfn2 coordinately regulate mitochondrial fusion and are essential for embryonic development. *J. Cell Biol.* **160**, 189–200 (2003).
- Chambers, S. M. *et al.* Highly efficient neural conversion of human ES and iPS cells by dual inhibition of SMAD signaling. *Nat. Biotechnol.* **27**, 275–280 (2009).
- Manuel, M. N., Mi, D., Mason, J. O. & Price, D. J. Regulation of cerebral cortical neurogenesis by the Pax6 transcription factor. *Front. Cell Neurosci.* **9**, 70 (2015).
- Shen, L., Nam, H. S., Song, P., Moore, H. & Anderson, S. A. FoxG1 haploinsufficiency results in impaired neurogenesis in the postnatal hippocampus and contextual memory deficits. *Hippocampus* **16**, 875–890 (2006).
- Polo-Parada, L., Bose, C. M., Plattner, F. & Landmesser, L. T. Distinct roles of different neural cell adhesion molecule (NCAM) isoforms in synaptic maturation revealed by analysis of NCAM 180 kDa isoform-deficient mice. *J. Neurosci.* **24**, 1852–1864 (2004).
- Cheng, A., Hou, Y. & Mattson, M. P. Mitochondria and neuroplasticity. *ASN. Neuro.* **2**, e00045 (2010).
- Tanaka, A. *et al.* Proteasome and p97 mediate mitophagy and degradation of mitofusins induced by Parkin. *J. Cell Biol.* **191**, 1367–1380 (2010).
- Greber, B. *et al.* FGF signalling inhibits neural induction in human embryonic stem cells. *EMBO J.* **30**, 4874–4884 (2011).
- Son, M. J. *et al.* Mitofusins deficiency elicits mitochondrial metabolic reprogramming to pluripotency. *Cell Death Differ.* **22**, 1957–1969 (2015).
- Garcia, S. J., Seidler, F. J., Crumpton, T. L. & Slotkin, T. A. Does the developmental neurotoxicity of chlorpyrifos involve glial targets? Macromolecule synthesis, adenylyl cyclase signaling, nuclear transcription factors, and formation of reactive oxygen in C6 glioma cells. *Brain Res.* **891**, 54–68 (2001).
- Basha, M. & Poojary, A. Cold stress offered modulation on chlorpyrifos toxicity in aging rat central nervous system. *Toxicol. Int.* **19**, 173–181 (2012).
- Yamada, S. *et al.* Tributyltin induces mitochondrial fission through Mfn1 degradation in human induced pluripotent stem cells. *Toxicol. In Vitro.* **34**, 257–263 (2016).
- Leboucher, G. P. *et al.* Stress-induced phosphorylation and proteasomal degradation of mitofusin 2 facilitates mitochondrial fragmentation and apoptosis. *Mol. Cell* **47**, 547–557 (2012).
- Yue, W. *et al.* A small natural molecule promotes mitochondrial fusion through inhibition of the deubiquitinase USP30. *Cell Res.* **24**, 482–496 (2014).
- Park, Y. Y., Nguyen, O. T., Kang, H. & Cho, H. MARCH5-mediated quality control on acetylated Mfn1 facilitates mitochondrial homeostasis and cell survival. *Cell Death Dis.* **5**, e1172 (2014).
- Chen, K. H. *et al.* Dysregulation of HSG triggers vascular proliferative disorders. *Nat. Cell Biol.* **6**, 872–883 (2004).
- Chen, K. H. *et al.* Role of mitofusin 2 (Mfn2) in controlling cellular proliferation. *FASEB J.* **28**, 382–394 (2014).
- Yu, Z. P., Matsuoka, M., Wispriyono, B., Iryo, Y. & Igisu, H. Activation of mitogen-activated protein kinases by tributyltin in CCRF-CEM cells: role of intracellular Ca<sup>2+</sup>. *Toxicol. Appl. Pharmacol.* **168**, 200–207 (2000).
- Pizzo, P., Drago, I., Filadi, R. & Pozzan, T. Mitochondrial Ca<sup>2+</sup> homeostasis: mechanism, role, and tissue specificities. *Pflugers Arch.* **464**, 3–17 (2012).

39. Danesin, C. & Houart, C. A. Fox stops the Wnt: implications for forebrain development and diseases. *Curr. Opin. Genet. Dev.* **22**, 323–330 (2012).
40. Georgala, P. A., Carr, C. B. & Price, D. J. The role of Pax6 in forebrain development. *Dev. Neurobiol.* **71**, 690–709 (2011).
41. Tuoc, T. C. *et al.* Selective cortical layering abnormalities and behavioral deficits in cortex-specific Pax6 knock-out mice. *J. Neurosci.* **29**, 8335–8349 (2009).
42. Tian, C. *et al.* Foxg1 has an essential role in postnatal development of the dentate gyrus. *J. Neurosci.* **32**, 2931–2949 (2012).
43. Chen, X. P., Chen, W. Z., Wang, F. S. & Liu, J. X. Selective cognitive impairments are related to selective hippocampus and prefrontal cortex deficits after prenatal chlorpyrifos exposure. *Brain Res.* **1474**, 19–28 (2012).
44. Li, K. *et al.* Differentiation of pluripotent stem cells for regenerative medicine. *Biochem. Biophys. Res. Commun.* **471**, 1–4 (2016).
45. Nakagawa, M. *et al.* Generation of induced pluripotent stem cells without Myc from mouse and human fibroblasts. *Nat. Biotechnol.* **26**, 101–106 (2008).
46. Fan, X., Hussien, R. & Brooks, G. A. H<sub>2</sub>O<sub>2</sub>-induced mitochondrial fragmentation in C2C12 myocytes. *Free Radic. Biol. Med.* **49**, 1646–1654 (2010).
47. Hirata, N. *et al.* Sphingosine-1-phosphate promotes expansion of cancer stem cells via S1PR3 by a ligand-independent Notch activation. *Nat. Commun.* **5**, 4806 (2014).
48. Kanda, Y. *et al.* Reactive oxygen species mediate adipocyte differentiation in mesenchymal stem cells. *Life Sci.* **89**, 250–258 (2011).
49. Yamada, S. *et al.* NAD-dependent isocitrate dehydrogenase as a novel target of tributyltin in human embryonic carcinoma cells. *Sci. Rep.* **4**, 5952 (2014).

### Acknowledgements

This work was supported by a Health and Labour Sciences Research Grant from the Ministry of Health, Labour, and Welfare, Japan (#H25-Kagaku-Ippan-002 and #H28-Kagaku-Ippan-003 to Y.Ka.), a Grant-in-Aid for Scientific Research from the Ministry of Education, Culture, Sports, Science, and Technology, Japan (#26293056 and #26670041 to Y.Ka.), the Japan Agency for Medical Research and Development, AMED (#15mk0104053h0101 and #16mk0104027j0002 to Y.S.), and a grant from the Smoking Research Foundation (Y.Ka.).

### Author Contributions

Y.S. and Y.Ka. planned the project. S.Y. performed most of the experiments. S.Y. and Y.Ka. wrote the manuscript. Y.Ku. and D.Y. provided technical advices. All authors reviewed the manuscript.

### Additional Information

**Supplementary information** accompanies this paper at <http://www.nature.com/srep>

**Competing financial interests:** The authors declare no competing financial interests.

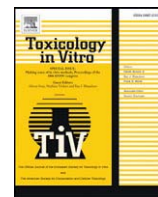
**How to cite this article:** Yamada, S. *et al.* Chlorpyrifos inhibits neural induction via Mfn1-mediated mitochondrial dysfunction in human induced pluripotent stem cells. *Sci. Rep.* **7**, 40925; doi: 10.1038/srep40925 (2017).

**Publisher's note:** Springer Nature remains neutral with regard to jurisdictional claims in published maps and institutional affiliations.



This work is licensed under a Creative Commons Attribution 4.0 International License. The images or other third party material in this article are included in the article's Creative Commons license, unless indicated otherwise in the credit line; if the material is not included under the Creative Commons license, users will need to obtain permission from the license holder to reproduce the material. To view a copy of this license, visit <http://creativecommons.org/licenses/by/4.0/>

© The Author(s) 2017



## Tributyltin induces mitochondrial fission through Mfn1 degradation in human induced pluripotent stem cells



Shigeru Yamada<sup>a</sup>, Miki Asanagi<sup>a,b</sup>, Naoya Hirata<sup>a</sup>, Hiroshi Itagaki<sup>b</sup>, Yuko Sekino<sup>a</sup>, Yasunari Kanda<sup>a,\*</sup>

<sup>a</sup> Division of Pharmacology, National Institute of Health Sciences, Japan

<sup>b</sup> Faculty of Engineering, Department of Materials Science and Engineering, Yokohama National University, Japan

### ARTICLE INFO

#### Article history:

Received 31 October 2015

Received in revised form 2 March 2016

Accepted 24 April 2016

Available online 29 April 2016

#### Keywords:

Induced pluripotent stem cells

Mitochondrial fission

Mitofusin

Tributyltin

### ABSTRACT

Organotin compounds, such as tributyltin (TBT), are well-known endocrine disruptors. TBT is also known to cause various forms of cytotoxicity, including neurotoxicity and immunotoxicity. However, TBT toxicity has not been identified in normal stem cells. In the present study, we examined the effects of TBT on cell growth in human induced pluripotent stem cells (iPSCs). We found that exposure to nanomolar concentrations of TBT decreased intracellular ATP levels and inhibited cell viability in iPSCs. Because TBT suppressed energy production, which is a critical function of the mitochondria, we further assessed the effects of TBT on mitochondrial dynamics. Staining with MitoTracker revealed that nanomolar concentrations of TBT induced mitochondrial fragmentation. TBT also reduced the expression of mitochondrial fusion protein mitofusin 1 (Mfn1), and this effect was abolished by knockdown of the E3 ubiquitin ligase membrane-associated RING-CH 5 (MARCH5), suggesting that nanomolar concentrations of TBT could induce mitochondrial dysfunction via MARCH5-mediated Mfn1 degradation in iPSCs. Thus, mitochondrial function in normal stem cells could be used to assess cytotoxicity associated with metal exposure.

© 2016 Elsevier Ltd. All rights reserved.

### 1. Introduction

Human induced pluripotent stem cells (iPSCs), which possess self-renewal and multipotent differentiation properties, are expected to have applications in drug discovery and drug safety assessment (Nakamura et al., 2014; Takahashi et al., 2007). Growing evidence suggests that iPSCs can also provide a unique platform for assessing chemical-induced toxicities in various tissues, such as the brain (He et al., 2012; Kumar et al., 2015). Thus, it is necessary to elucidate the mechanisms mediating the cytotoxic effects of different chemicals during embryonic development in stem cells.

Organotin compounds, such as tributyltin (TBT), are also associated with various developmental, neurological, immunological, and metabolic effects (Kotake, 2012). Although the use of TBT has already been restricted, butyltin compounds, including TBT, have been reported to be still present at concentrations between 50 and 400 nM in human blood (Whalen et al., 1999). Therefore, the mechanisms through which nanomolar concentrations of TBT cause cytotoxicity should be elucidated using undifferentiated normal stem cells, which is the most suitable platform for toxicological analysis.

Several studies have revealed the cytotoxic effects of nanomolar concentrations of TBT in stem cells. For example, nanomolar concentrations of TBT activate retinoid X receptor (RXR) and/or peroxisome

proliferator-activated receptor  $\gamma$  (PPAR $\gamma$ ), thereby enhancing adipocyte differentiation in adipose-derived stromal stem cells (ADSCs) (Kirchner et al., 2010). In rat mesencephalic neural stem cells, transcriptome analysis after induction of TBT-dependent apoptosis revealed changes in the expression levels of genes involved in Ca<sup>2+</sup> mobilization, retinoic acid signaling, and apoptosis (Suzuki and Ishido, 2011). We previously reported that nanomolar concentrations of TBT mediate mitochondrial dysfunction and inhibit the growth of human embryonic carcinoma NT2/D1 cells (Yamada et al., 2015). Thus, we hypothesized that nanomolar concentrations of TBT could also affect mitochondria in human iPSCs.

Mitochondria exhibit continuous changes in morphology through fusion and fission (van der Bliek et al., 2013; Youle and van der Bliek, 2012). Under normal circumstances, mitochondria fuse together, forming excessive tubular networks (mitochondrial fusion). In contrast, under stress conditions, mitochondrial networks convert into large numbers of small fragments with punctate morphology (mitochondrial fission). These mitochondrial dynamics play a key role in the maintenance of mitochondrial functions, such as ATP production. Mitochondrial morphology is strictly regulated by fission (fission protein 1 [Fis1] and dynamin-related protein 1 [Drp1]) and fusion (mitofusin 1 and 2 [Mfn1, Mfn2] and optic atrophy 1 [Opa1]) factors (Fischer et al., 2012). Several reports have described mitochondrial fragmentation induced by chemical exposure. For example, CGP37157, an inhibitor of mitochondrial calcium efflux, mediates mitochondrial fission through Mfn1 degradation via the E3 ubiquitin ligase membrane-associated RING-CH 5

\* Corresponding author at: 1-18-1, Kamiyoga, Setagaya-ku, 158-8501, Japan.  
E-mail address: [kanda@nihs.go.jp](mailto:kanda@nihs.go.jp) (Y. Kanda).

(MARCH5) in prostate cancer cells (Choudhary et al., 2014). Another study showed that doxorubicin induces proteasomal degradation of Mfn2, which facilitates mitochondrial fragmentation and apoptosis in sarcoma U2OS cells (Lebouche et al., 2012).

In the present study, we investigated the cytotoxic effects of nanomolar concentrations of TBT in iPSCs. Our results showed that exposure to 50 nM TBT decreased intracellular ATP levels and inhibited cell growth. Moreover, TBT exposure induced Mfn1 degradation and mitochondrial fragmentation through a MARCH5-dependent mechanism. Thus, nanomolar concentrations of TBT induce toxicity through impairment of mitochondrial quality control in human iPSCs.

## 2. Materials and methods

### 2.1. Chemicals and reagents

TBT was obtained from Tokyo Chemical Industry (Tokyo, Japan). Tin acetate (TA), rosiglitazone (RGZ), and carbonyl cyanide m-chlorophenyl hydrazone (CCCP) were obtained from Sigma-Aldrich (St. Louis, MO, USA). All other reagents were of analytical grade and were obtained from commercial sources.

### 2.2. Cell culture

We used the human iPSC line 253G1 (Riken BRC Cell Bank, Tsukuba, Ibaraki, Japan), which was established through retroviral transduction of Oct3/4, Sox2, and Klf4 into adult human dermal fibroblasts (Nakagawa et al., 2008). The cells were cultured under feederless conditions using human embryonic stem cell (ESC)-qualified Matrigel (BD Biosciences, San Jose, CA, USA) and TeSR-E8 medium (Stemcell Technologies, Vancouver, BC, Canada) at 37 °C in an atmosphere containing 5% CO<sub>2</sub>. For passage, iPSC colonies were dissociated into single cells using Accumax (Innovative Cell Technologies, San Diego, CA, USA) and cultured in a TeSR-E8 medium supplemented with the Rho-kinase (ROCK) inhibitor Y-27632 (Wako, Tokyo, Japan).

### 2.3. Cell proliferation assay

Cell viability was measured using CellTiter 96 AQueous One Solution Cell Proliferation Assays (Promega, Madison, WI, USA), according to the manufacturer's instructions. Briefly, iPSCs were seeded into 96-well plates and exposed to different concentrations of TBT. After exposure to TBT, One Solution Reagent was added to each well, and the plate was incubated at 37 °C for another 2 h. Absorbance was measured at 490 nm using an iMark microplate reader (Bio-Rad, Hercules, CA, USA).

### 2.4. Measurement of intracellular ATP levels

The intracellular ATP content was measured using an ATP Determination Kit (Life Technologies, Carlsbad, CA, USA), according to the manufacturer's protocol. Briefly, the cells were washed and lysed with 0.1% Triton X-100/PBS. The resulting cell lysates were added to a reaction mixture containing 0.5 mM D-luciferin, 1 mM DTT, and 1.25 µg/mL luciferase and incubated for 30 min at room temperature. Luminescence was measured using a Fluoroskan Ascent FL microplate reader (Thermo Fisher Scientific, Waltham, MA, USA). The luminescence intensities were normalized to the total protein content.

### 2.5. Measurement of mitochondrial membrane potential (MMP)

A Cell Meter JC-10 Mitochondrial Membrane Potential Assay Kit (AAT Bioquest, Sunnyvale, CA, USA) was used to detect MMP. Briefly, the cells were suspended in a staining buffer containing JC-10 and incubated for 20 min at room temperature. After treatment of the cells with chemicals, a FACS Aria II cell sorter (BD Biosciences) was used to

measure the fluorescence intensity ratio, that is, JC-aggregate (F-590)/JC-monomer (F-535).

### 2.6. Assessment of mitochondrial fusion

After the cells were treated with TBT (50 nM, 72 h), they were fixed with 4% paraformaldehyde and stained with 50 nM MitoTracker Red CMXRos (Cell Signaling Technology, Danvers, MA, USA) and 5 µg/mL Hoechst 33342 (Sigma-Aldrich). Changes in mitochondrial morphology were observed using a confocal laser microscope (Nikon A1). Images (n = 5) were taken of random fields, and the number of cells displaying mitochondrial fusion (<10% punctiform) was counted in each image, as previously reported (Fan et al., 2010).

### 2.7. Real-time polymerase chain reaction (PCR)

Total RNA was isolated from iPSCs using TRIzol reagent (Life Technologies), and quantitative real-time reverse transcription (RT)-PCR was performed using a QuantiTect SYBR Green RT-PCR Kit (Qiagen, Valencia, CA, USA) on an ABI PRISM 7900HT sequence detection system (Applied Biosystems, Foster City, CA, USA) as previously reported (Hirata et al., 2014). Relative changes in transcript levels were normalized to the mRNA levels of glyceraldehyde-3-phosphate dehydrogenase (GAPDH). The following primer sequences were used for real-time PCR analysis: *Nanog*, forward, 5'-CAGAAGCCTCAGCACCTAC-3' and reverse, 5'-ATTGTCCAGTCTGGTTGC-3'; *Oct3/4*, forward, 5'-ACATCAAAGCTC TGCAGAAAGAA-3' and reverse, 5'-CCAGTTCCTTGGCCTGGTT-3'; *Drp1*, forward, 5'-TGGGGCCGACATCA-3' and reverse, 5'-GCTCTGCGTCCCA CTACGA-3'; *Fis1*, forward, 5'-TACGTCCGCGGTTGCT-3' and reverse, 5'-CCAGTTCCTTGGCCTGGTT-3'; *Mfn1*, forward, 5'-GGCATCTGTGGCCG AGTT-3' and reverse, 5'-ATTATGCTAAGTCTCCGCTCCAA-3'; *Mfn2*, forward, 5'-GCTCGGAGGCACATGAAAGT-3' and reverse, 5'-ATCACGGTGC TCTTCCATT-3'; *Opa1*, forward, 5'-GTGCTGCCCGCTAGAAA-3' and reverse, 5'-TGACAGGCACCCGACTACTAGT-3'; *GAPDH*, forward, 5'-GTCTCC TCTGACTTCAACAGCG-3' and reverse, 5'-ACCACCCTGTGCTGTAGCC AA-3'.

### 2.8. Western blot analysis

Western blot analysis was performed as previously reported (Kanda et al., 2011). Briefly, the cells were lysed with a Cell Lysis Buffer (Cell Signaling Technology). The proteins were then separated by sodium dodecyl sulfate-polyacrylamide gel electrophoresis (SDS-PAGE) and electrophoretically transferred to Immobilon-P membranes (Millipore, Billerica, MA, USA). The membranes were probed with anti-Drp1 monoclonal antibodies (1:1000; Cell Signaling Technology), anti-Fis1 polyclonal antibodies (1:200; Santa Cruz Biotechnology, Santa Cruz, CA, USA), anti-Mfn1 polyclonal antibodies (1:1000; Cell Signaling Technology), anti-Mfn2 monoclonal antibodies (1:1000; Cell Signaling Technology), anti-Opa1 monoclonal antibodies (1:1000; BD Biosciences), and anti-β-actin monoclonal antibodies (1:5000; Sigma-Aldrich). The membranes were then incubated with secondary antibodies against rabbit or mouse IgG conjugated to horseradish peroxidase (Cell Signaling Technology). The bands were visualized using an ECL Western Blotting Analysis System (GE Healthcare, Buckinghamshire, UK), and images were acquired using an LAS-3000 Imager (Fujifilm, Tokyo, Japan).

### 2.9. Gene knockdown by shRNA

Knockdown experiments were performed using Mfn1 shRNA lentiviruses from Sigma-Aldrich (MISSION shRNA), as previously reported (Yamada et al., 2014). A scrambled hairpin sequence was used as a negative control. Briefly, the cells were infected with the viruses at a multiplicity of infection of 1 in the presence of 8 mg/mL hexadimethrine bromide (Sigma-Aldrich) for 24 h. The cells were then subjected to

selection with 1  $\mu\text{g}/\text{mL}$  puromycin for 24 h and cultured for an additional 72 h prior to functional analyses.

### 2.10. Gene knockdown by siRNA

Double-stranded RNA oligonucleotides (siRNAs) against MARCH5 and appropriate control scrambled siRNA were purchased from Life Technologies. The siRNAs were transfected into iPSCs using DharmaFECT1 (Dharmacon, Lafayette, CO, USA) as previously described (Kinehara et al., 2013).

### 2.11. Statistical analysis

All data were presented as means  $\pm$  standard deviations (SDs). Analysis of variance (ANOVA) followed by post-hoc Tukey test was used to analyze data involving more than two samples. For comparisons between two samples, Student's *t*-tests were used. Differences with *P*-values of less than 0.05 were considered statistically significant.

## 3. Results

### 3.1. Cytotoxic effects of TBT in iPSCs

To examine whether TBT was cytotoxic in iPSCs, we studied the effects of TBT on cell proliferation in iPSCs. Treatment with TBT reduced cell viability in a dose-dependent manner (Fig. 1A and B). The  $\text{LC}_{50}$  for TBT was 77 nM in iPSCs. Moreover, almost all cells were detached from the culture dish at more than 200 nM TBT. In contrast, exposure to TA, which is less toxic, had little effect at any concentration tested (Fig. 1A and B). We next examined whether TBT affected pluripotency. The expression levels of the undifferentiated markers Nanog and

Oct3/4 were not changed by TBT (Fig. 1C). Because cell growth requires ATP as a source of energy in iPSCs, we examined intracellular ATP content in the cells. We found that treatment with 50 nM TBT reduced the ATP content of the cells (Fig. 1D). We confirmed that 0.1  $\mu\text{M}$  CCCP, which functions as a mitochondrial uncoupler, also decreased ATP levels. In contrast, TA had little effect. These data suggest that exposure to 50 nM TBT reduces cell growth without inhibiting iPSC pluripotency.

### 3.2. Effects of TBT on mitochondrial function in iPSCs

Because TBT inhibited ATP production, we investigated MMP, as an important parameter of mitochondrial function, during TBT treatment in iPSCs. MMP was decreased by 50 nM TBT for 1 h (Fig. 2A). In contrast, TA had little effect on MMP. We further examined the generation of reactive oxygen species (ROS), which affect MMP and are related to mitochondrion-mediated cell damage (Park et al., 2005), using 2',7'-dichlorodihydrofluorescein (DCFH). TBT at 50 nM did not affect the ROS level (Fig. S1). In contrast, hydrogen peroxide ( $\text{H}_2\text{O}_2$ ) as a positive control promoted the generation of ROS, which was attenuated by *N*-acetylcysteine treatment. Because morphological changes in mitochondria are closely related to energy supply and MMP maintenance (Youle and van der Bliek, 2012), we focused on mitochondrial dynamics in iPSCs. After TBT exposure, we observed fragmented mitochondria with punctate morphology (Fig. 2B). Furthermore, TBT significantly decreased the number of cells exhibiting mitochondrial fusion (Fig. 2C). As expected, fragmented mitochondria were also observed following CCCP treatment (Fig. S2). In contrast, TA exposure did not affect mitochondrial morphology. Taken together, these results suggest that nanomolar concentrations of TBT induce mitochondrial dysfunction, such as MMP depolarization and mitochondrial fragmentation, in iPSCs.

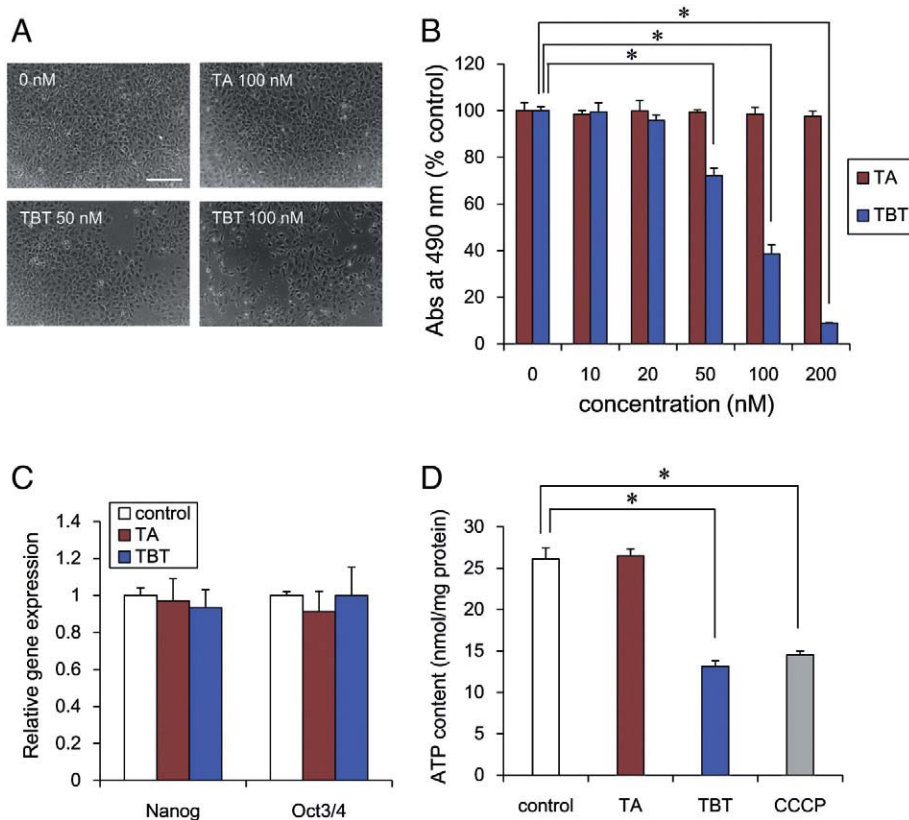


**Fig. 1.** TBT induces cytotoxic effects in iPSCs. (A) Cells were seeded in 96-well plates and exposed to different concentrations of TBT for 72 h. Phase-contrast photomicrographs of iPSCs were captured after exposure to TBT or TA at 0, 50, and 100 nM. Bar = 100  $\mu\text{m}$ . (B) Cell viability in the presence of TBT or TA was examined using CellTiter 96 AQueous One Solution Cell Proliferation Assays. (C) After exposure to 50 nM TBT or TA for 72 h, the expression of undifferentiated marker genes (*Nanog* and *Oct3/4*) was analyzed by real-time PCR. (D) The intracellular ATP content was determined in the lysed cells. Data represent the mean  $\pm$  SD ( $n = 3$ ). \* $P < 0.05$  using ANOVA with post-hoc Tukey test.

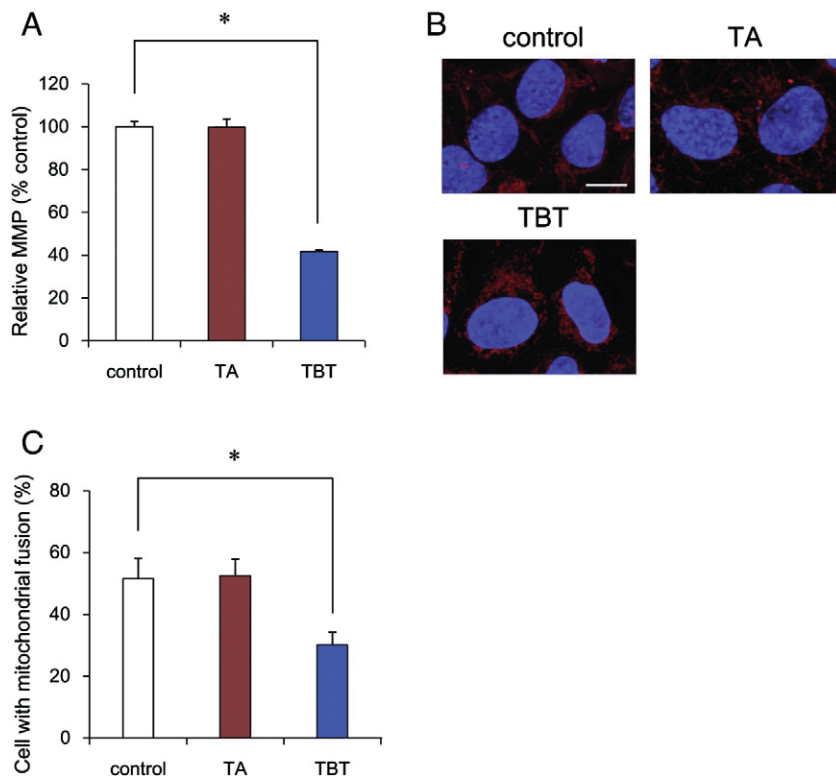


**Fig. 2.** TBT affects several mitochondrial functions in iPSCs. (A) Cells were stained with JC-10 for 20 min and exposed to 50 nM TBT or TA for an additional 1 h. The MMP of JC-10-labeled cells was analyzed by flow cytometry. (B) Cells were exposed to 50 nM TBT or TA for 72 h and then stained with MitoTracker Red CMXRos and Hoechst 33342. Mitochondrial morphology was observed by confocal laser microscopy. Bar = 10 μm. (C) The number of cells with mitochondrial fusion (<10% punctiform) was counted in each image. Data represent the mean ± SD (n = 5). \*P < 0.05 using ANOVA with post-hoc Tukey test.

### 3.3. TBT exposure induced mitochondrial fission via the reduction of Mfn1 protein in iPSCs

To examine the molecular mechanisms through which TBT induces mitochondrial fragmentation, we assessed the effects of TBT on the expression of mitochondrial fission (*Fis1* and *Drp1*) and fusion genes (*Mfn1*, *Mfn2*, and *OPA1*). Real-time PCR analysis showed that the expression of each gene was not altered by TBT exposure (Fig. 3A). Interestingly, western blot analysis revealed that TBT significantly decreased only Mfn1 protein levels. In contrast, the expression levels of other factors, including Mfn2, were not changed (Fig. 3B and C). To confirm the involvement of Mfn1 in the fragmentation of mitochondria, we performed knockdown (KD) of *Mfn1* using lentivirus-delivered shRNAs. Real-time PCR analysis showed that the KD efficiency was approximately 60% (Fig. 3D), which was similar to that reported in previous KD studies (Son et al., 2015). Similar to TBT exposure, Mfn1 KD induced mitochondrial fragmentation (Fig. 3E and F). These data suggest that TBT-induced mitochondrial fragmentation is caused by reduction of Mfn1 protein levels.

### 3.4. MARCH5 KD abolished TBT-induced Mfn1 reduction in iPSCs

To investigate whether Mfn1 reduction triggered by TBT occurred through an E3 ubiquitin ligase-dependent mechanism, we performed KD of MARCH5 by siRNA. Real-time PCR analysis showed that the KD efficiency of MARCH5 was approximately 70% (Fig. 4A). Western blot analysis revealed that MARCH5 KD increased basal Mfn1 levels and further abolished TBT-induced Mfn1 reduction (Fig. 4B and C). In contrast, Mfn2 protein levels were not recovered by MARCH5 KD. Because the gene expression of Mfn1 was not affected by TBT exposure, Mfn1 reduction was thought to be caused by MARCH5-mediated degradation, independent of gene downregulation. Taken together, these

data suggest that MARCH5 mediates TBT-induced Mfn1 degradation in iPSCs.

## 4. Discussion

In the present study, we demonstrated that nanomolar concentrations of TBT targeted mitochondrial quality control in human iPSCs. We showed that exposure to nanomolar concentrations of TBT induced Mfn1 degradation through the E3 ubiquitin ligase MARCH5, thereby promoting mitochondrial fragmentation. These negative effects of TBT on mitochondrial quality control could inhibit ATP production and cell growth.

Our results showed that treatment with more than 200 nM TBT caused almost complete detachment of human iPSCs from the culture dish (Fig. 1). Previous studies have shown that micromolar concentrations of TBT induce apoptosis in various cell types, such as human amnion cells (Zhu et al., 2007), hepatocytes (Grondin et al., 2007), and neutrophils (Lavastre and Girard, 2002). Compared to somatic cells, immature cells tend to be highly sensitive to TBT exposure. Therefore, analysis of TBT sensitivity using iPSCs, iPSC-neural progenitor cells, and iPSC-neurons might provide interesting insights into the mechanisms of TBT toxicity. Previous reports have shown that iPSC-derived cells are immature compared with human naïve neural cells and do not form neural networks (Belinsky et al., 2011). Therefore, further studies are required to elucidate the mechanisms of TBT neurotoxicity using iPSCs and to optimize the types of iPSC-derived cells.

We also showed that the stemness properties of iPSCs were maintained after TBT exposure, whereas cell growth was reduced (Fig. 1). Mitochondria have been reported to be in a morphologically and functionally immature state in iPSCs, with poorly developed cristae and more fragmented structures than those observed in somatic cells (Wanet et al., 2015). Mfn1 and Mfn2 have been shown to constitute a new barrier to reprogramming because Mfn1/2 ablation facilitates the

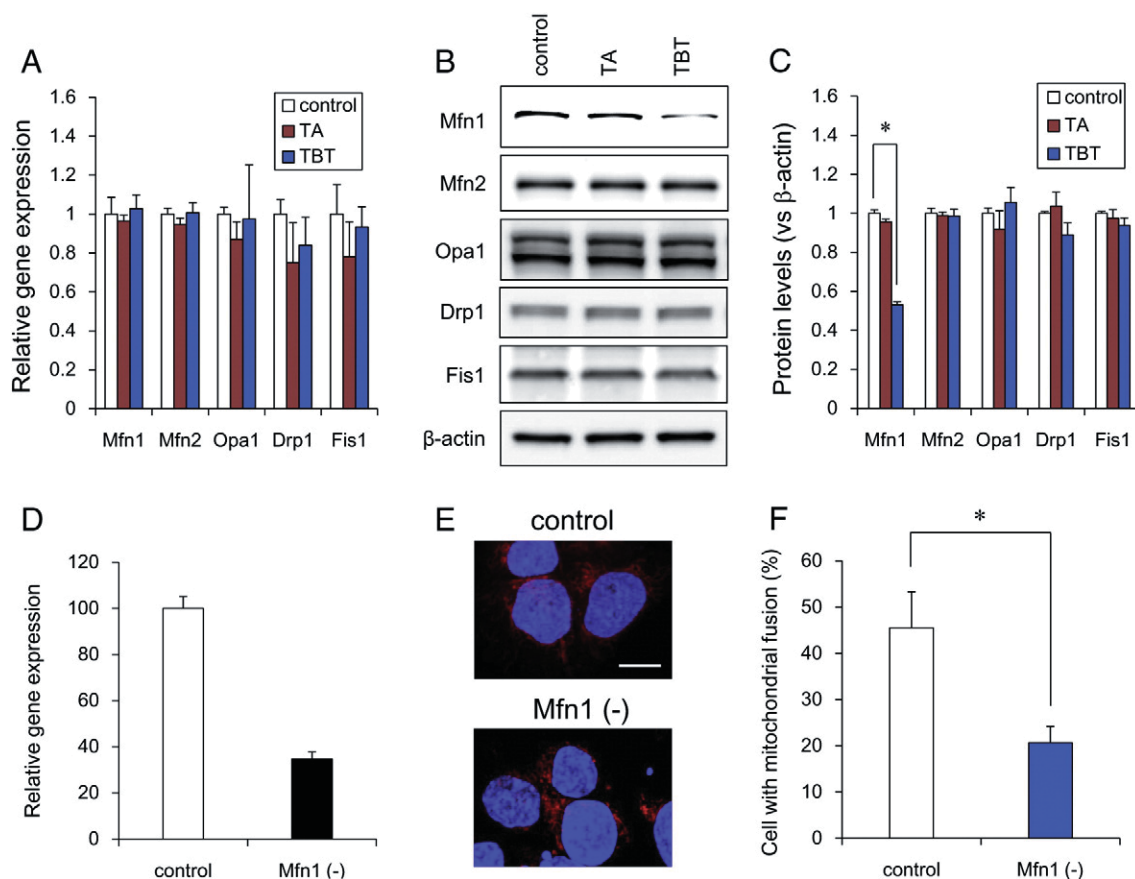


**Fig. 3.** TBT induces mitochondrial fission via decreased Mfn1 protein levels in iPSCs. (A) After exposure to 50 nM TBT or TA for 72 h, the expression of mitochondrial genes was analyzed by real-time PCR. (B) After exposure to 50 nM TBT or TA for 72 h, the expression of mitochondrial proteins was analyzed by western blotting using anti-Drp1, anti-Fis1, anti-Mfn1, anti-Mfn2, anti-Opa1, or anti- $\beta$ -actin antibodies. (C) The relative densities of bands were quantified with ImageJ software. Relative changes in expression were determined by normalization to  $\beta$ -actin. (D) After introduction of lentivirus-delivered shRNAs against *Mfn1* to the cells, the expression of *Mfn1* was analyzed by real-time PCR. (E) *Mfn1*-KD cells were stained with MitoTracker Red CMXRos and Hoechst 33342. Mitochondrial morphology was observed by confocal laser microscopy. Bar = 10  $\mu$ m. (F) The number of cells with mitochondrial fusion (<10% punctiform) was counted in each image. Data represent the mean  $\pm$  SD ( $n = 5$ ). \* $P < 0.05$  using ANOVA with post-hoc Tukey test.

induction of pluripotency through the restructuring of mitochondrial dynamics and bioenergetics (Son et al., 2015). Moreover, MARCH5 has been shown to be involved in maintaining the pluripotency of mouse embryonic stem cells through protein kinase A (PKA)-extracellular signal-regulated kinase (ERK) signaling (Gu et al., 2015). Thus, MARCH5-Mfn1 might be involved in maintenance of embryonic stemness through mitochondrial fragmentation in iPSCs. Previous study has reported that Mfn1 knockout results in embryonic lethality of homozygous mutants (Chen et al., 2003). Moreover, Mfn1-deficient embryonic cells have dramatically fragmented mitochondria. Taken together, these data indicate that Mfn1-mediated mitochondrial dynamics might regulate embryonic development. Further studies are needed to determine whether MARCH5-mediated Mfn1 degradation plays a role in the maintenance of stemness properties.

Our data suggest that nanomolar concentrations of TBT could induce mitochondrial fission through MARCH5-mediated Mfn1 degradation (Figs. 2–4). Consistent with our data, chemical stressors have been reported to cause mitochondrial fission through proteasomal degradation of Mfn1 and/or Mfn2 (Choudhary et al., 2014; Leboucher et al., 2012). In addition, Mfn1 or Mfn2 deficiency in cells is known to result in severe cellular defects, including decreased ATP content and poor cell growth (Chen et al., 2005; Yue et al., 2014). Our Mfn1 KD studies indicated that Mfn1 degradation was sufficient to promote mitochondrial dysfunction; therefore, TBT-induced Mfn1 degradation might mediate mitochondrial fragmentation, decrease ATP levels, and inhibit iPSC growth. Although Mfn2 is also involved in mitochondrial fission and energy supply (Chen et al., 2005; Leboucher et al., 2012; Yue et al., 2014),

our results indicated that TBT specifically targeted Mfn1, not Mfn2. Regarding this apparent TBT specificity, MARCH5 has been reported to selectively degrade Mfn1 among all mitochondrial proteins, including Mfn2 (Park et al., 2014). This selectivity of MARCH5 toward Mfn1 was also confirmed by our recovery studies of TBT-induced Mfn1 degradation using MARCH5-KD cells. Thus, exposure to nanomolar concentrations of TBT might specifically target Mfn1 via MARCH5 in iPSCs. In future studies, it will be necessary to investigate the specific mechanisms underlying TBT-induced Mfn1 degradation via MARCH5, a process that results in mitochondrial fission and dysfunction.

Herein, we found that TBT targeted the mitochondrial energy supply in iPSCs. Although mitochondrial energy production is more efficient than glycolysis, embryonic cells such as iPSCs are known to rely mainly on glycolysis rather than the mitochondrial system for ATP production (Varum et al., 2011). We previously reported that nanomolar concentrations of TBT inhibit glucose uptake and cause growth arrest in human embryonic carcinoma NT2/D1 cells (Yamada et al., 2013). Further studies should determine whether glycolysis is also targeted by TBT in iPSCs.

In summary, our results demonstrated a novel mechanism underlying the cytotoxicity of nanomolar TBT levels in iPSCs. Recently, significant progress has been made in the induction of differentiation of pluripotent stem cells into a variety of cell types (Li et al., 2016). Thus, further studies are needed to evaluate the toxicities and developmental effects of TBT on somatic cells present in human adults. The chemical sensitivity and broad utility of iPSCs in toxicological studies of TBT may enable the discovery of versatile toxicity evaluation markers,

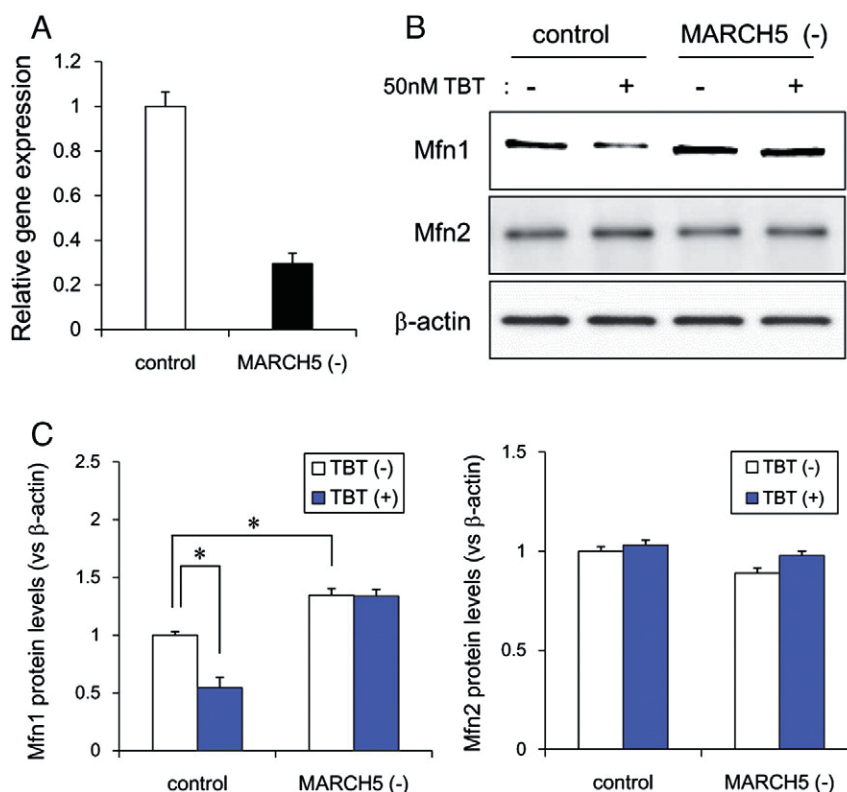


**Fig. 4.** MARCH5 KD abolishes TBT-induced Mfn1 degradation in iPSCs. (A) Cells were transfected with siRNA targeting MARCH5 or a scrambled siRNA (control), and the relative expression of MARCH5 was measured using real-time PCR. (B) After exposure to 50 nM TBT or TA for 72 h in siRNA-transfected cells, protein levels of Mfn1 and Mfn2 were examined by western blotting using anti-Mfn1, anti-Mfn2, or anti-β-actin antibodies. (C) The relative densities of bands were quantified with ImageJ software. Relative changes in expression were determined by normalization to β-actin. Data represent the mean ± SD (n = 3). \**P* < 0.05 using Student's *t*-tests (A) or ANOVA with post hoc Tukey tests (C).

which could facilitate the development of a platform for chemical validation by providing simple, reproducible, and cost-effective tools.

#### Conflict of interest

The authors declare that there are no conflicts of interest.

#### Transparency document

The Transparency document associated with this article can be found, in online version.

#### Acknowledgments

This work was supported by a Health and Labour Sciences Research Grant from the Ministry of Health, Labour, and Welfare, Japan (#H25-Kagaku-Ippan-002 and #H28-Kagaku-Ippan-003 to Y. Kanda), a Grant-in-Aid for Scientific Research from the Ministry of Education, Culture, Sports, Science, and Technology, Japan (#26293056 and #26670041 to Y. Kanda), the Research on Regulatory Harmonization and Evaluation of Pharmaceuticals, Medical Devices, Regenerative and Cellular Therapy Products, Gene Therapy Products, and Cosmetics from Japan Agency for Medical Research and Development, AMED (#15mk0104053h0101 to Y. Sekino), and a grant from the Smoking Research Foundation (Y. Kanda).

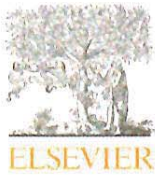
#### Appendix A. Supplementary data

Supplementary data to this article can be found online at <http://dx.doi.org/10.1016/j.tiv.2016.04.013>.

#### References

- Belinsky, G.S., Moore, A.R., Short, S.M., Rich, M.T., Antic, S.D., 2011. Physiological properties of neurons derived from human embryonic stem cells using a dibutyl cyclic AMP-based protocol. *Stem Cells Dev.* 20, 1733–1746.
- Chen, H., Detmer, S.A., Ewald, A.J., Griffin, E.E., Fraser, S.E., Chan, D.C., 2003. Mitofusins Mfn1 and Mfn2 coordinately regulate mitochondrial fusion and are essential for embryonic development. *J. Cell Biol.* 160, 189–200.
- Chen, H., Chomyn, A., Chan, D.C., 2005. Disruption of fusion results in mitochondrial heterogeneity and dysfunction. *J. Biol. Chem.* 280, 26185–26192.
- Choudhary, V., Kaddour-Djebbar, I., Alaisami, R., Kumar, M.V., Bollag, W.B., 2014. Mitofusin 1 degradation is induced by a disruptor of mitochondrial calcium homeostasis, CGP37157: a role in apoptosis in prostate cancer cells. *Int. J. Oncol.* 44, 1767–1773.
- Fan, X., Hussien, R., Brooks, G.A., 2010. H<sub>2</sub>O<sub>2</sub>-induced mitochondrial fragmentation in C2C12 myocytes. *Free Radic. Biol. Med.* 49, 1646–1654.
- Fischer, F., Hamann, A., Osiewicz, H.D., 2012. Mitochondrial quality control: an integrated network of pathways. *Trends Biochem. Sci.* 37, 284–292.
- Gronin, M., Marion, M., Denizeau, F., Averill-Bates, D.A., 2007. Tributyltin induces apoptotic signaling in hepatocytes through pathways involving the endoplasmic reticulum and mitochondria. *Toxicol. Appl. Pharmacol.* 222, 57–68.
- Gu, H., Li, Q., Huang, S., Lu, W., Cheng, F., Gao, P., Wang, C., Miao, L., Mei, Y., Wu, M., 2015. Mitochondrial E3 ligase March5 maintains stemness of mouse ES cells via suppression of ERK signalling. *Nat. Commun.* 6, 7112.
- He, X., Imanishi, S., Sone, H., Nagano, R., Qin, X.Y., Yoshinaga, J., Akanuma, H., Yamane, J., Fujibuchi, W., Ohsako, S., 2012. Effects of methylmercury exposure on neuronal differentiation of mouse and human embryonic stem cells. *Toxicol. Lett.* 212, 1–10.
- Hirata, N., Yamada, S., Shoda, T., Kurihara, M., Sekino, Y., Kanda, Y., 2014. Sphingosine-1-phosphate promotes expansion of cancer stem cells via S1PR3 by a ligand-independent Notch activation. *Nat. Commun.* 5, 4806.
- Kanda, Y., Hinata, T., Kang, S.W., Watanabe, Y., 2011. Reactive oxygen species mediate adipocyte differentiation in mesenchymal stem cells. *Life Sci.* 89, 250–258.
- Kinehara, M., Kawamura, S., Tateyama, D., Suga, M., Matsumura, H., Mimura, S., Hirayama, N., Hirata, M., Uchio-Yamada, K., Kohara, A., Yanagihara, K., Furue, M.K., 2013. Protein kinase C regulates human pluripotent stem cell self-renewal. *PLoS One* 8, e54122.
- Kirchner, S., Kieu, T., Chow, C., Casey, S., Blumberg, B., 2010. Prenatal exposure to the environmental obesogen tributyltin predisposes multipotent stem cells to become adipocytes. *Mol. Endocrinol.* 24, 526–539.
- Kotake, Y., 2012. Molecular mechanisms of environmental organotin toxicity in mammals. *Biol. Pharm. Bull.* 35, 1876–1880.

- Kumar, V., Jahan, S., Singh, S., Khanna, V.K., Pant, A.B., 2015. Progress toward the development of in vitro model system for chemical-induced developmental neurotoxicity: potential applicability of stem cells. *Arch. Toxicol.* 89, 265–267.
- Lavastre, V., Girard, D., 2002. Tributyltin induces human neutrophil apoptosis and selective degradation of cytoskeletal proteins by caspases. *J. Toxic. Environ. Health A* 65, 1013–1024.
- Leboucher, G.P., Tsai, Y.C., Yang, M., Shaw, K.C., Zhou, M., Veenstra, T.D., Glickman, M.H., Weissman, A.M., 2012. Stress-induced phosphorylation and proteasomal degradation of mitofusin 2 facilitates mitochondrial fragmentation and apoptosis. *Mol. Cell* 47, 547–557.
- Li, K., Kong, Y., Zhang, M., Xie, F., Liu, P., Xu, S., 2016. Differentiation of pluripotent stem cells for regenerative medicine. *Biochem. Biophys. Res. Commun.* 471, 1–4.
- Nakagawa, M., Koyanagi, M., Tanabe, K., Takahashi, K., Ichisaka, T., Aoi, T., Okita, K., Mochizuki, Y., Takizawa, N., Yamanaka, S., 2008. Generation of induced pluripotent stem cells without Myc from mouse and human fibroblasts. *Nat. Biotechnol.* 26, 101–106.
- Nakamura, Y., Matsuo, J., Miyamoto, N., Ojima, A., Ando, K., Kanda, Y., Sawada, K., Sugiyama, A., Sekino, Y., 2014. Assessment of testing methods for drug-induced repolarization delay and arrhythmias in an iPSC cell-derived cardiomyocyte sheet: multi-site validation study. *J. Pharm. Sci.* 124, 494–501.
- Park, M.T., Kim, M.J., Kang, Y.H., Choi, S.Y., Lee, J.H., Choi, J.A., Kang, C.M., Cho, C.K., Kang, S., Bae, S., Lee, Y.S., Chung, H.Y., Lee, S.J., 2005. Phytosphingosine in combination with ionizing radiation enhances apoptotic cell death in radiation-resistant cancer cells through ROS-dependent and -independent AIF release. *Blood* 105, 1724–1733.
- Park, Y.Y., Nguyen, O.T., Kang, H., Cho, H., 2014. MARCH5-mediated quality control on acetylated Mfn1 facilitates mitochondrial homeostasis and cell survival. *Cell Death Dis.* 5, e1172.
- Son, M.J., Kwon, Y., Son, M.Y., Seol, B., Choi, H.S., Ryu, S.W., Choi, C., Cho, Y.S., 2015. Mitofusins deficiency elicits mitochondrial metabolic reprogramming to pluripotency. *Cell Death Differ.* 10, 1–13.
- Suzuki, J.S., Ishido, M., 2011. Transcriptome of tributyltin-induced apoptosis of the cultured rat mesencephalic neural stem cells. *Toxicology* 287, 61–68.
- Takahashi, K., Tanabe, K., Ohnuki, M., Narita, M., Ichisaka, T., Tomoda, K., Yamanaka, S., 2007. Induction of pluripotent stem cells from adult human fibroblasts by defined factors. *Cell* 131, 861–872.
- van der Bliek, A.M., Shen, Q., Kawajiri, S., 2013. Mechanisms of mitochondrial fission and fusion. *Cold Spring Harb. Perspect. Biol.* 5 (pii: a011072).
- Varum, S., Rodrigues, A.S., Moura, M.B., Momcilovic, O., Easley IV., C.A., Ramalho-Santos, J., Van Houten, B., Schatten, G., 2011. Energy metabolism in human pluripotent stem cells and their differentiated counterparts. *PLoS One* 6, e20914.
- Wanet, A., Arnould, T., Najimi, M., Renard, P., 2015. Connecting mitochondria, metabolism, and stem cell fate. *Stem Cells Dev.* 24, 1957–1971.
- Whalen, M.M., Loganathan, B.G., Kannan, K., 1999. Immunotoxicity of environmentally relevant concentrations of butyltins on human natural killer cells in vitro. *Environ. Res.* 81, 108–116.
- Yamada, S., Kotake, Y., Sekino, Y., Kanda, Y., 2013. AMP-activated protein kinase-mediated glucose transport as a novel target of tributyltin in human embryonic carcinoma cells. *Metalomics* 5, 484–491.
- Yamada, S., Kotake, Y., Demizu, Y., Kurihara, M., Sekino, Y., Kanda, Y., 2014. NAD-dependent isocitrate dehydrogenase as a novel target of tributyltin in human embryonic carcinoma cells. *Sci. Rep.* 4, 5952.
- Yamada, S., Kotake, Y., Nakano, M., Sekino, Y., Kanda, Y., 2015. Tributyltin induces mitochondrial fission through NAD-IDH dependent mitofusin degradation in human embryonic carcinoma cells. *Metalomics* 7, 1240–1246.
- Youle, R.J., van der Bliek, A.M., 2012. Mitochondrial fission, fusion, and stress. *Science* 337, 1062–1065.
- Yue, W., Chen, Z., Liu, H., Yan, C., Chen, M., Feng, D., Yan, C., Wu, H., Du, L., Wang, Y., Liu, J., Huang, X., Xia, L., Liu, L., Wang, X., Jin, H., Wang, J., Song, Z., Hao, X., Chen, Q., 2014. A small natural molecule promotes mitochondrial fusion through inhibition of the deubiquitinase USP30. *Cell Res.* 24, 482–496.
- Zhu, X., Xing, M., Lou, J., Wang, X., Fu, W., Xu, L., 2007. Apoptotic related biochemical changes in human amnion cells induced by tributyltin. *Toxicology* 230, 45–52.



# Nicotine induces mitochondrial fission through mitofusin degradation in human multipotent embryonic carcinoma cells

Naoya Hirata<sup>a,1</sup>, Shigeru Yamada<sup>a,1</sup>, Miki Asanagi<sup>a,b</sup>, Yuko Sekino<sup>a</sup>, Yasunari Kanda<sup>a,\*</sup>

<sup>a</sup> Division of Pharmacology, National Institute of Health Sciences, Japan

<sup>b</sup> Faculty of Engineering, Department of Materials Science and Engineering, Yokohama National University, Japan

## ARTICLE INFO

### Article history:

Received 5 January 2016

Accepted 10 January 2016

Available online xxx

### Keywords:

Embryonic cells

Cigarette smoking

Nicotine

Mitochondrial fission

Mitofusin

## ABSTRACT

Nicotine is considered to contribute to the health risks associated with cigarette smoking. Nicotine exerts its cellular functions by acting on nicotinic acetylcholine receptors (nAChRs), and adversely affects normal embryonic development. However, nicotine toxicity has not been elucidated in human embryonic stage. In the present study, we examined the cytotoxic effects of nicotine in human multipotent embryonic carcinoma cell line NT2/D1. We found that exposure to 10  $\mu$ M nicotine decreased intracellular ATP levels and inhibited proliferation of NT2/D1 cells. Because nicotine suppressed energy production, which is a critical mitochondrial function, we further assessed the effects of nicotine on mitochondrial dynamics. Staining with MitoTracker revealed that 10  $\mu$ M nicotine induced mitochondrial fragmentation. The levels of the mitochondrial fusion proteins, mitofusins 1 and 2, were also reduced in cells exposed to nicotine. These nicotine effects were blocked by treatment with mecamylamine, a nonselective nAChR antagonist. These data suggest that nicotine degrades mitofusin in NT2/D1 cells and thus induces mitochondrial dysfunction and cell growth inhibition in a nAChR-dependent manner. Thus, mitochondrial function in embryonic cells could be used to assess the developmental toxicity of chemicals.

© 2016 Published by Elsevier Inc.

## 1. Introduction

Growing evidence suggest that maternal smoking during pregnancy is related to adverse neurodevelopmental outcomes in the offspring, including lower intelligence quotients and deficits in learning and memory [1,2]. Nicotine is a naturally occurring alkaloid that is present in tobacco leaves and is considered to contribute to the negative effects of cigarette smoking on health [2,3]. Nicotine exerts its cellular functions by activating nicotinic acetylcholine receptors (nAChRs), which are heterodimers composed of combinations of different types of  $\alpha$  subunit ( $\alpha 1$ – $\alpha 10$ ) and  $\beta$  subunit ( $\beta 1$ – $\beta 4$ ) [4].  $\alpha 8$ -nAChR has not been identified in human. Recent studies have shown that nAChRs are present in a variety of cells, such as cancer cells, vascular smooth muscle, and neural cells [3–6]. Activation of nAChRs by nicotine promotes the release of various neurotransmitters (including dopamine, norepinephrine, acetylcholine, glutamate) [7]. Altered regulation of neurotransmitter levels can adversely affect key events in normal brain

development, such as the formation of neural circuits and neurotransmitter systems [7,8]. Therefore, it is necessary to elucidate the cytotoxic effects of nicotine on embryonic development.

Nicotine toxicity has been reported to affect mitochondrial function both *in vitro* and *in vivo*. For example, nicotine exposure alters mitochondrial membrane potential (MMP), increases an oxidative stress, and induces apoptosis in colon adenocarcinoma HCT-116 cell [9]. Another study has shown that nicotine exposure reduced the activity of an enzyme in the pancreatic mitochondrial respiratory chain, and impaired glucose-stimulated insulin secretion in neonatal rats [10]. However, the precise mechanisms underlying the effects of nicotine on mitochondrial function remain largely unknown.

Growing evidence suggest that mitochondria undergo continuous morphological dynamics involving fusion and fission cycles. These dynamics play a key role in maintenance of normal mitochondrial functions, such as ATP production [11]. Mitochondrial fusion and fission are regulated by several GTPases. Mitofusin 1 and 2 (Mfn1, 2) and optic atrophy 1 (Opa1) induce fusion of the outer and inner mitochondrial membranes, respectively [12,13]. In contrast, dynamin-related protein 1 (Drp1) is a cytoplasmic protein that assembles into rings surrounding the outer mitochondrial

\* Corresponding author. 1-18-1, Kamiyoga, Setagaya-ku, 158-8501, Japan.

E-mail address: [kanda@nihs.go.jp](mailto:kanda@nihs.go.jp) (Y. Kanda).

<sup>1</sup> Equally contributed.

<http://dx.doi.org/10.1016/j.bbrc.2016.01.063>

0006-291X/© 2016 Published by Elsevier Inc.

membrane, where it interacts with fission protein 1 (Fis1) to promote fission [14,15]. For example, pigment epithelium-derived factor is reported to improve mitochondrial function by stabilizing mitochondrial fusion in retinal pigment epithelial cells [16]. In contrast, the anti-tumor agent, doxorubicin, facilitates mitochondrial fragmentation and apoptosis by promoting Mfn2 degradation in sarcoma U2OS cells [17].

In the present study, we hypothesized a possible link between nicotine toxicity and mitochondrial function in human multipotent NT2/D1 cells, which have neural differentiation capability. Our results showed that exposure to 10  $\mu$ M nicotine decreased intracellular ATP levels and inhibited cell growth. Moreover, nicotine exposure induced Mfn degradation and mitochondrial fragmentation via nicotinic acetylcholine receptors (nAChRs). Thus, nicotine induces toxicity through impairment of mitochondrial quality control in human NT2/D1 cells.

## 2. Materials and methods

### 2.1. Cell culture

The human multipotent embryonal carcinoma NT2/D1 cells were obtained from the American Type Culture Collection (Manassas, VA, USA). SH-SY5Y cells were obtained from European Collection of Animal Cell Culture (Salisbury, Wiltshire, UK). The cells were cultured in Dulbecco's modified Eagle's medium (DMEM; Sigma–Aldrich, St. Louis, MO, USA) supplemented with 10% fetal bovine serum (FBS; Biological Industries, Ashrat, Israel) and 0.05 mg/ml penicillin-streptomycin mixture (Life Technologies, Carlsbad, CA, USA) at 37 °C in the presence of 5% CO<sub>2</sub>.

### 2.2. Cell proliferation assay

Cell viability was measured using the CellTiter 96 Aqueous One Solution Cell Proliferation Assay (Promega, Madison, WI, USA), as previously described [18]. Briefly, NT2/D1 cells were seeded into 96-well plate and exposed to different concentrations of nicotine. After exposure to nicotine, One Solution Reagent was added to each well, and the plate was incubated at 37 °C for another 2 h. Absorbance was measured at 490 nm by iMark microplate reader (Bio-Rad, Hercules, CA, USA).

### 2.3. Measurement of intracellular ATP levels

The intracellular ATP content was measured using the ATP Determination Kit (Life Technologies), as previously described [19]. Briefly, the cells were washed and lysed with phosphate-buffered saline containing 0.1% Triton X-100. The resulting cell lysates were added to a reaction mixture containing 0.5 mM D-luciferin, 1 mM dithiothreitol, and 1.25  $\mu$ g/ml luciferase and incubated for 30 min at room temperature. Luminescence was measured using a Wallac1420ARVO fluoroscan (Perkin–Elmer, Waltham, MA, USA). The luminescence intensities were normalized to the total protein content.

### 2.4. Assessment of mitochondrial fusion

After treatment with nicotine (10  $\mu$ M, 24 h), cells were fixed with 4% paraformaldehyde and stained with 50 nM MitoTracker Red CMXRos (Cell Signaling Technology, Danvers, MA, USA) and 0.1  $\mu$ g/ml 4',6-diamidino-2-phenylindole (DAPI; Dojin, Kumamoto, Japan). Changes in mitochondrial morphology were observed using a confocal laser microscope (Nikon A1). Images (n 3–7) of random fields were taken, and the number of cells displaying mitochondrial fusion (<10% punctiform) was counted in each image, as previously

described [20]. The number of cells showing mitochondrial fission was calculated by subtracting the number of cells with mitochondrial fusion from the total cell number.

### 2.5. Real-time PCR

Total RNA was isolated from NT2/D1 cells using TRIzol reagent (Life Technologies), and quantitative real-time reverse transcription (RT)-PCR with QuantiTect SYBR Green RT-PCR Kit (QIAGEN, Valencia, CA, USA) was performed using an ABI PRISM 7900HT sequence detection system (Applied Biosystems, Foster City, CA, USA) as previously described [21]. The relative change in the amount of transcript was normalized to the mRNA levels of glyceraldehyde-3-phosphate dehydrogenase (GAPDH). The following primer sequences were used for real-time PCR analysis: *nAChR $\alpha$ 1*, forward, 5'-CTGGACCTACGCGCTCT-3' and reverse, 5'-CGCTGCATGACGAAGTGGT-3'; *nAChR $\alpha$ 2*, forward, 5'-ACACTTCAGCGTGGTGATTG-3' and reverse, 5'-CCACTCCTGTTTAGCCAGAC-3'; *nAChR $\alpha$ 3*, forward, 5'-ACCTGTGGCTCAAGCAAATCT-3' and reverse, 5'-GCAGGGACACGCATGAACT-3'; *nAChR $\alpha$ 4*, forward, 5'-GGAGGGCGTCCAGTACATTG-3' and reverse, 5'-GAA-GATGCGGTCGATGACCA-3'; *nAChR $\alpha$ 5*, forward, 5'-AGATGGAACCTGATGACTATGGT-3' and reverse, 5'-AAACGTCATCTGCATTATCAAAC-3'; *nAChR $\alpha$ 6*, forward, 5'-GGCAGGGATTCCCTTCATGGG-3' and reverse, 5'-GCCTCTCTCAGTTGCACAG-3'; *nAChR $\alpha$ 7*, forward, 5'-CATGGCCTTCTCGGTCTTCA-3' and reverse, 5'-CACGGCCTCCACGAAGTT-3'; *nAChR $\alpha$ 10*, forward, 5'-CAGATGCTACTACGATGGG-3' and reverse, 5'-GGGAAGGCTGCTACATCCA-3'; *nAChR $\beta$ 1*, forward, 5'-TGACACTACTACTACTACCCA-3' and reverse, 5'-AGAACCACGACACTAAGGATGA-3'; *nAChR $\beta$ 2*, forward, 5'-GGTGACAGTACAGCTTATGGTG-3' and reverse, 5'-AGGCGATAATCTCCCACTCC-3'; *nAChR $\beta$ 3*, forward, 5'-TGCTGGTCTCATCGTCTTG-3' and reverse, 5'-GCATCTTATTTCGGCGATTGA-3'; *nAChR $\beta$ 4*, forward, 5'-CAGCTTATCAGCGTGAATGAGC-3' and reverse, 5'-GTCAGGCGGTAATCAGTCCAT-3'; *Drp1*, forward, 5'-TGGGCGCCGACATCA-3' and reverse, 5'-GCTCTCGGTCCCCTACTACGA-3'; *Fis1*, forward, 5'-TACGTCGCGGGTTGCT-3' and reverse, 5'-CCAGTTCCTTGGCCTGGTT-3'; *Mfn1*, forward, 5'-GGCATCTGTGGCCGAGTT-3' and reverse, 5'-ATTATGCTAAGTCTCCGCTCCA-3'; *Mfn2*, forward, 5'-GCTCGGAGGCACATGAAAGT-3' and reverse, 5'-ATCACGGTGCTCTCCCAIT-3'; *Opa1*, forward, 5'-GTGCTGCCCGCTAGAAA-3' and reverse, 5'-TGA-CAGGCACCCGTACTCAGT-3'; *GAPDH*, forward, 5'-GTCTCTTGACTTCAACAGCG-3' and reverse, 5'-ACCACCTGTTGCTGTAGCCAA-3'.

### 2.6. Western blot analysis

Western blot analysis was performed as previously reported [22]. Briefly, the cells were lysed with Cell Lysis Buffer (Cell Signaling Technology). The proteins were then separated by sodium dodecyl sulfate-polyacrylamide gel electrophoresis (SDS-PAGE) and electrophoretically transferred to Immobilon-P (Millipore, Billerica, MA, USA). The membranes were probed with anti-Drp1 monoclonal antibodies (1:1000; Cell Signaling Technology), anti-Fis1 polyclonal antibodies (1:200; Santa Cruz Biotechnology, Santa Cruz, CA, USA), anti-Mfn1 polyclonal antibodies (1:1000; Cell Signaling Technology), anti-Mfn2 monoclonal antibodies (1:1000; Cell Signaling Technology), anti-Opa1 monoclonal antibodies (1:1000; BD Biosciences), and anti- $\beta$ -actin monoclonal antibodies (1:5000; Sigma–Aldrich). The membranes were then incubated with secondary antibodies against rabbit or mouse IgG conjugated to horseradish peroxidase (Cell Signaling Technology). The bands were visualized using the ECL Western Blotting Analysis System (GE

Healthcare, Buckinghamshire, UK), and images were acquired using a LAS-3000 Imager (FUJIFILM UK Ltd., Systems, Bedford, UK).

## 2.7. Chemicals and reagents

Nicotine was obtained from Wako Pure Chemicals (Osaka, Japan). Mecamylamine hydrochloride (MCA) and m-chlorophenylhydrazine (CCCP) were obtained from Sigma–Aldrich.

## 2.8. Statistical analysis

All data were presented as means  $\pm$  S.D. ANOVA followed by post hoc Fisher test was used to analyze data in Fig. 1A and B and Figs. 2–4B. Student's *t*-test was used to analyze data in Fig. 4C. *P*-

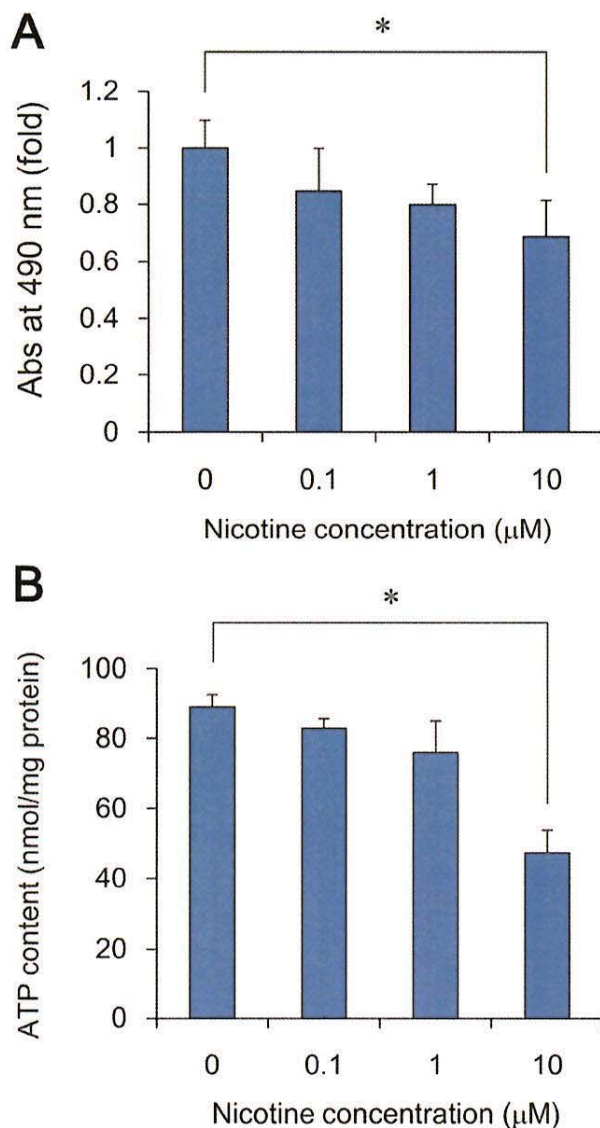


**Fig. 1.** Nicotine inhibits cell proliferation via intracellular ATP decrease in NT2/D1 cells. A. Cells were exposed to different concentrations of nicotine for 72 h. Cell viability was examined using the CellTiter 96 Aqueous One Solution Cell Proliferation Assay. B. After treatment with different concentrations of nicotine for 24 h, intracellular ATP content was determined in cell lysates. Data represent the mean  $\pm$  SD (n 3). \**P* < 0.05.

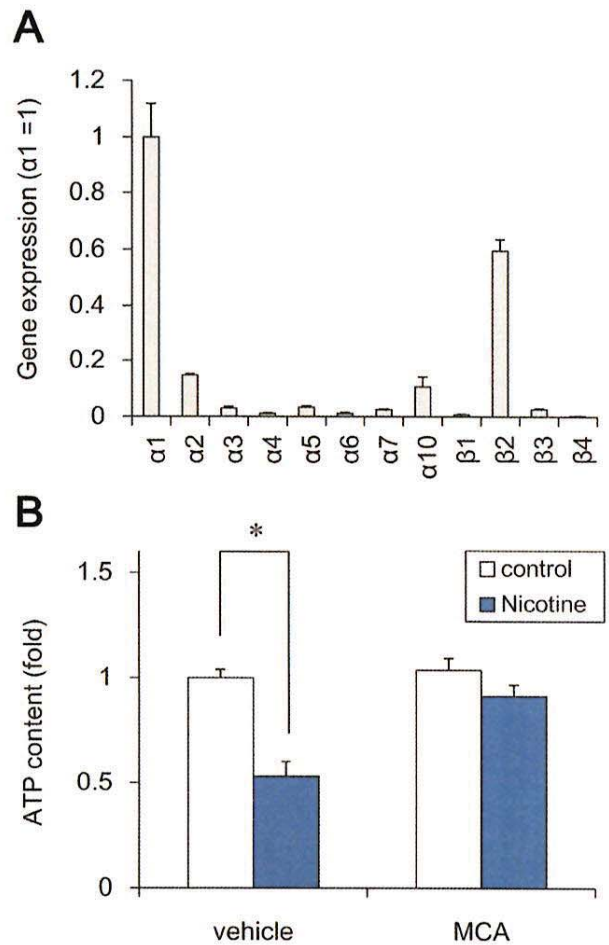


**Fig. 2.** Nicotine reduces intracellular ATP levels via nAChRs in NT2/D1 cells. A. Expression of AChR subtypes was analyzed by real-time PCR in NT2/D1 cells. The relative changes were determined by normalizing with GAPDH. B. After treatment with 10  $\mu\text{M}$  nicotine and/or 30  $\mu\text{M}$  MCA for 24 h, intracellular ATP content was determined in cell lysates. Data represent the mean  $\pm$  SD (n 3). \**P* < 0.05.

values less than 0.05 were considered to be statistically significant.

## 3. Results

### 3.1. Cytotoxic effects of nicotine in NT2/D1 cells

To examine the effects of nicotine on human multipotent embryonic cells, we exposed the cells to different concentrations of nicotine for 72 h and measured cell viability by MTT assay using human multipotent embryonic carcinoma NT2/D1 cells, which have an ability to differentiate into neuronal cells. We found that treatment with 10  $\mu\text{M}$  nicotine significantly inhibited cell proliferation (Fig. 1A). Similarly, exposure to 10  $\mu\text{M}$  nicotine significantly reduced the ATP content of the cells (Fig. 1B). To further investigate whether the nicotine effects are selective for undifferentiated cells, we used human SH-SY5Y neuroblastoma cells. We found that exposure to 10  $\mu\text{M}$  nicotine had little effect on proliferation and ATP content of SH-SY5Y cells (Fig. S1).

We next examined the nAChR mRNA levels by real-time PCR and confirmed that nAChR subtypes except  $\alpha 9$ -nAChR were expressed in NT2/D1 cells (Fig. 2A). To examine whether the inhibition of ATP

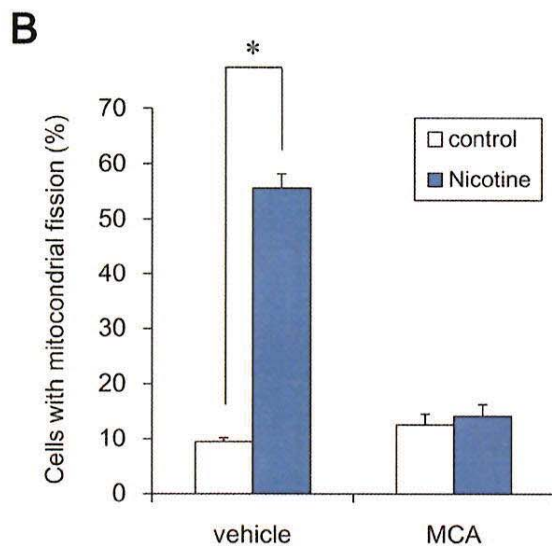
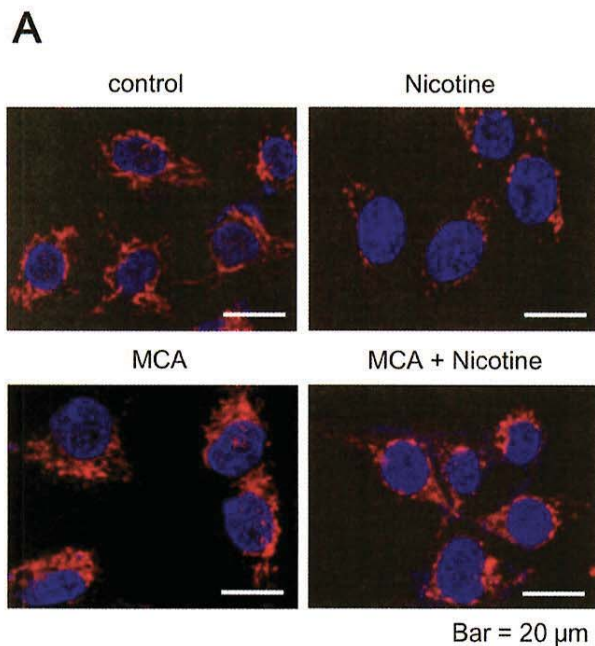


**Fig. 3.** Nicotine induces mitochondrial fission via nAChRs in NT2/D1 cells. A. Cells were exposed to 10  $\mu$ M nicotine, in the presence or absence of 30  $\mu$ M MCA, for 24 h. The cells were stained with MitoTracker Red CMXRos and DAPI and mitochondrial morphology was observed by confocal laser microscopy. Bar 20  $\mu$ m. B. The number of cells showing mitochondrial fission (<10% punctiform) was counted in three independent captured images. The number of cells showing mitochondrial fission was calculated by subtracting the number of cells with mitochondrial fusion from the total cell number. \* $P < 0.05$ .

production is mediated via the nAChRs, we tested the effect of nAChR antagonist on the ATP content. As shown in Fig. 2B, a non-selective nAChR antagonist mecamylamine (MCA) abolished the nicotine-induced reduction of ATP content. MCA alone did not affect the ATP level. These data suggest that nicotine decreases the ATP content via its nAChR and inhibits cell proliferation in NT2/D1 cells.

### 3.2. Effects of nicotine on mitochondrial morphology in NT2/D1 cells

Mitochondrial function, including ATP production, are maintained by mitochondrial fusion and fission [11]. Since nicotine reduced intracellular ATP levels, we next focused on the mitochondrial dynamics in NT2/D1 cells. Nicotine exposure (10  $\mu$ M, 24 h) significantly increased the number of fragmented mitochondria with punctate morphology, as compared to the level observed in untreated control cells (Fig. 3). Moreover, MCA abolished this nicotine-induced mitochondrial fragmentation (Fig. 3). MCA alone did not affect mitochondrial dynamics. In contrast to NT2/D1 cells, nicotine did not significantly affect the mitochondrial dynamics in SH-SY5Y neuroblastoma cells (Fig. S1). These results suggest that nicotine induces mitochondrial fission via nAChRs in NT2/D1 cells.

### 3.3. Nicotine reduces Mfn1 and Mfn2 protein levels in NT2/D1 cells

To examine the molecular mechanism by which nicotine induces mitochondrial fragmentation, we assessed its effects on mitochondrial fission (Fis1, Drp1) and fusion genes (Mfn1, Mfn2, Opa1). Real-time PCR analysis showed that each gene expression was not significantly altered by nicotine exposure (Fig. 4A). Interestingly, western blot analysis revealed that nicotine did significantly decrease the levels of Mfn1 and Mfn2 proteins (Fig. 4B and C). In contrast, the levels of other proteins, including Fis1, Drp1, and Opa1, were not affected by nicotine. These data suggest that nicotine-induced mitochondrial fragmentation is caused by the degradation of Mfn1 and Mfn2 proteins.

## 4. Discussion

In the present study, we demonstrated that exposure to micromolar levels of nicotine impairs mitochondrial quality control in human multipotent embryonic carcinoma cells. Exposure to nicotine induces nAChR-dependent degradation of Mfn1 and Mfn2, thereby promoting mitochondrial fragmentation. These negative nAChR-mediated effects of nicotine on mitochondrial quality control could inhibit ATP production and cell viability.

Undifferentiated embryonic cells may tend to be sensitive to the growth inhibitory effects of nicotine, whereas proliferative and protective effects of nicotine have been described in more developed somatic cells [23–27]. Our studies showed that treatment with 10  $\mu$ M nicotine reduces cell growth in human embryonic cells (Fig. 1), whereas the growth of human neuroblastoma SH-SY5Y cells is not affected (Fig. S1). Previous study has also shown that exposure to more than 1.8  $\mu$ M nicotine inhibits cell adhesion and induces apoptosis in human embryonic stem cells [28]. The concentrations of nicotine tested in our study were relevant to the circulating levels of nicotine in cigarette smokers, which have been reported to range from 10 nM to 10  $\mu$ M [29]; these have the potential to inhibit the growth of embryonic cells. In contrast to these growth inhibitory effects, nicotine is known to stimulate the proliferation of hematopoietic and neuronal progenitors [23–25]. In addition, nicotine is reported to protect rat basal forebrain neurons or rat hippocampal neurons from the cytotoxicity of  $\beta$ -amyloid protein [26,27]. Taken together, nicotine effects in undifferentiated embryonic cells contains different mechanisms from developed somatic cells. Therefore, further studies are required to elucidate the mechanism of cell stage-specific effects using embryonic and differentiated cells.

Our data suggest that nicotine induces mitochondrial fission through the degradation of Mfn1 and Mfn2 (Figs. 3 and 4). Consistent with this finding, chemical stressors have been reported

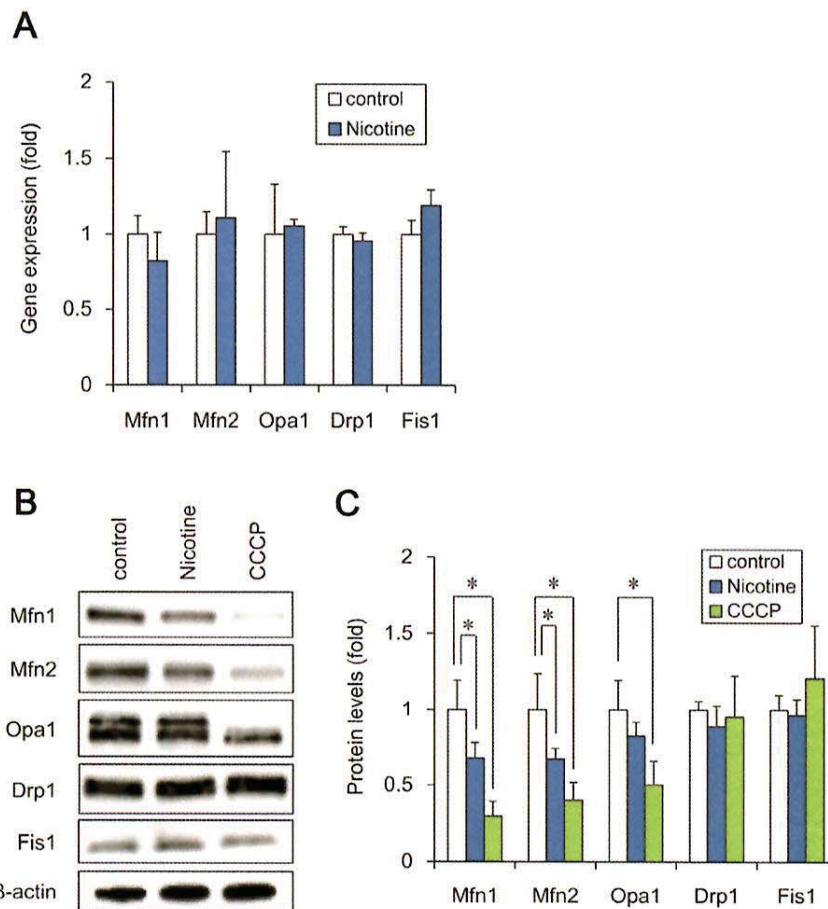


**Fig. 4.** Nicotine reduces Mfn1 and Mfn2 protein levels in NT2/D1 cells. **A.** After exposure to 10  $\mu$ M nicotine for 24 h, the expression of the indicated mitochondrial genes was analyzed by real-time PCR. The relative changes were determined by normalizing with GAPDH. **B.** After exposure to 10  $\mu$ M nicotine or 10  $\mu$ M CCCP for 24 h, the expression of mitochondrial proteins was analyzed by western blot using anti-Drp1, anti-Fis1, anti-Mfn1, anti-Mfn2, anti-Opa1, or anti- $\beta$ -actin antibodies. **C.** The band densities were analyzed by ImageJ software. Relative changes in expression were determined by normalization to  $\beta$ -actin. Data represent the mean  $\pm$  SD (n 3). \*P < 0.05.

to cause mitochondrial fission via Mfn degradation. For example, organotin compounds such as tributyltin induce proteasomal degradation of Mfn1 and Mfn2, which facilitates mitochondrial fragmentation and growth arrest in NT2/D1 cells [30,31]. Since nicotine showed similar effects in NT2/D1 cells, nicotine exposure may also degrade Mfn1 and Mfn2 via proteasome. Moreover, an inhibitor of mitochondrial calcium efflux, CGP37157, is reported to degrade Mfn1 via E3 ubiquitin ligase and induce mitochondrial fission in prostate cancer LNCaP cells [32]. Further studies will be necessary to determine whether ubiquitin ligases are involved in nicotine-induced Mfn1 and Mfn2 degradation in embryonic cells.

Our data suggest that nicotine toxicity is mediated by dysfunctional mitochondrial quality control, which occurs via a nAChR-dependent mechanism (Figs. 2 and 3). Nicotine has been reported to evoke extracellular calcium influx through plasma membrane nAChRs [4]. Moreover, a transient increase in intracellular calcium levels is known to cause mitochondrial calcium overload, which is followed by the depolarization of the mitochondrial membrane, resulting in a loss of MMP [33,34]. In other cell lines, MMP reduction is reported to induce the mitochondrial translocation of the E3 ubiquitin ligase, Parkin, which targets the Mfn protein for proteasomal degradation [35]. Therefore, nicotine may increase intracellular calcium entry via nAChRs, thus reducing the MMP and

inducing mitochondrial translocation of E3 ubiquitin ligases; this increases the proteasomal degradation of Mfn1 and Mfn2. Several reports indicate that knockdown of Mfn1 and Mfn2 in the cells induces mitochondrial fragmentation and shows severe cellular defects, including decreased ATP content and poor cell growth [36,37]. Especially, Mfn2 has been reported to be necessary for striatal axonal projections of midbrain dopamine neurons by the studies using dopamine neuron-specific Mfn2 knockout mice [38]. Taken together, Mfn1 and Mfn2 might be involved in several nAChR-mediated effects of nicotine, such as the reduction of ATP content, growth inhibition, and modulation of synaptic transmission. In future studies, it will be necessary to investigate the precise mechanism involved in nicotine-induced Mfn degradation, which results in mitochondrial fission and impaired function.

#### Conflict of interest

The authors declare that there are no conflicts of interest.

#### Acknowledgments

This work was supported by a Health and Labour Sciences Research Grant from the Ministry of Health, Labour and Welfare,

Please cite this article in press as: N. Hirata, et al., Nicotine induces mitochondrial fission through mitofusin degradation in human multipotent embryonic carcinoma cells, Biochemical and Biophysical Research Communications (2016), <http://dx.doi.org/10.1016/j.bbrc.2016.01.063>

1 Japan (#H25-Kagaku-Ippan-002 to Y. Kanda), a Grant-in-Aid for  
2 Scientific Research from the Ministry of Education, Culture, Sports,  
3 Science, and Technology, Japan (#26293056, #26670041 to Y.  
4 Kanda), the Research on Regulatory Harmonization and Evaluation  
5 of Pharmaceuticals, Medical Devices, Regenerative and Cellular  
6 Therapy Products, Gene Therapy Products, and Cosmetics from  
7 Japan Agency for Medical Research and development, AMED (to Y.  
8 Sekino), and a grant from the Smoking Research Foundation (Y.  
9 Kanda).

#### 10 Transparency document

11  
12  
13 Transparency document related to this article can be found  
14 online at <http://dx.doi.org/10.1016/j.bbrc.2016.01.063>.

#### 15 Appendix A. Supplementary data

16  
17  
18 Supplementary data related to this article can be found at [http://](http://dx.doi.org/10.1016/j.bbrc.2016.01.063)  
19 [dx.doi.org/10.1016/j.bbrc.2016.01.063](http://dx.doi.org/10.1016/j.bbrc.2016.01.063).

#### 20 References

- 21  
22  
23 [1] V.S. Knopik, Maternal smoking during pregnancy and child outcomes: real or  
24 spurious effect? *Dev. Neuropsychol.* 34 (2009) 1–36.  
25 [2] C.M. Tiesler, J. Heinrich, Prenatal nicotine exposure and child behavioural  
26 problems, *Eur. Child. Adolesc. Psychiatry* 23 (2014) 913–929.  
27 [3] B.M. Conti-Fine, D. Navaneetham, S. Lei, A.D. Maus, Neuronal nicotinic re-  
28 ceptors in non-neuronal cells: new mediators of tobacco toxicity? *Eur. J.*  
29 *Pharmacol.* 393 (2000) 279–284.  
30 [4] E.X. Albuquerque, E.F. Pereira, M. Alkondon, S.W. Rogers, Mammalian nicotinic  
31 acetylcholine receptors: from structure to function, *Physiol. Rev.* 89 (2009)  
32 73–120.  
33 [5] Y. Kanda, Y. Watanabe, Nicotine-induced vascular endothelial growth factor  
34 release via the EGFR-ERK pathway in rat vascular smooth muscle cells, *Life Sci.*  
35 80 (2007) 1409–1414.  
36 [6] N. Hirata, Y. Sekino, Y. Kanda, Nicotine increases cancer stem cell population  
37 in MCF-7 cells, *Biochem. Biophys. Res. Commun.* 403 (2010) 138–143.  
38 [7] N.L. Benowitz, Pharmacology of nicotine: addiction, smoking-induced disease,  
39 and therapeutics, *Annu. Rev. Pharmacol. Toxicol.* 49 (2009) 57–71.  
40 [8] J.B. Dwyer, S.C. McQuown, F.M. Leslie, The dynamic effects of nicotine on the  
41 developing brain, *Pharmacol. Ther.* 122 (2009) 125–139.  
42 [9] C.L. Crowley-Weber, K. Dvorakova, C. Crowley, H. Bernstein, C. Bernstein,  
43 H. Garewal, C.M. Payne, Nicotine increases oxidative stress, activates NF-  
44 kappaB and GRP78, induces apoptosis and sensitizes cells to genotoxic/  
45 xenobiotic stresses by a multiple stress inducer, deoxycholate: relevance to  
46 colon carcinogenesis, *Chem. Biol. Interact.* 145 (2003) 53–66.  
47 [10] J.E. Bruin, M.A. Petre, S. Raha, K.M. Morrison, H.C. Gerstein, A.C. Holloway,  
48 Fetal and neonatal nicotine exposure in wistar rats causes progressive  
49 pancreatic mitochondrial damage and beta cell dysfunction, *PLoS One* 3  
50 (2008) e3371.  
51 [11] R.J. Youle, A.M. van der Bliek, Mitochondrial fission, fusion, and stress, *Science*  
52 337 (2012) 1062–1065.  
53 [12] T. Koshiba, S.A. Detmer, J.T. Kaiser, H. Chen, J.M. McCaffery, D.C. Chan, Struc-  
54 tural basis of mitochondrial tethering by mitofusin complexes, *Science* 305  
55 (2004) 858–862.  
56 [13] S. Cipolat, O.M. De Brito, B. Dal Zilio, L. Scorrano, OPA1 requires mitofusin 1 to  
57 promote mitochondrial fusion, *Proc. Natl. Acad. Sci. U. S. A.* 101 (2004)  
15927–15932.  
58 [14] E. Smirnova, L. Griparic, D.-L. Shurland, A.M. van der Bliek, Dynamin-related  
59 protein Drp1 is required for mitochondrial division in mammalian cells, *Mol.*  
60 *Biol. Cell* 12 (2001) 2245–2256.  
61 [15] Y. Yoon, E.W. Krueger, B.J. Oswald, M.A. McNiven, The mitochondrial protein  
62 hFis1 regulates mitochondrial fission in mammalian cells through an inter-  
63 action with the dynamin-like protein DLP1, *Mol. Biol. Cell* 23 (2003)  
5409–5420.  
64 [16] Y. He, K.W. Leung, Y. Ren, J. Pei, J. Ge, J. Tombran-Tink, PEDF improves  
65 mitochondrial function in RPE cells during oxidative stress, *Investig. Oph-  
66 thalmol. Vis. Sci.* 55 (2014) 6742–6755.  
67 [17] G.P. LeBoucher, Y.C. Tsai, M. Yang, K.C. Shaw, M. Zhou, T.D. Veenstra,  
68 M.H. Glickman, A.M. Weissman, Stress-induced phosphorylation and protea-  
69 somal degradation of mitofusin 2 facilitates mitochondrial fragmentation and  
70 apoptosis, *Mol. Cell* 47 (2012) 547–557.  
71 [18] S. Yamada, Y. Kotake, Y. Sekino, Y. Kanda, AMP-activated protein kinase-  
72 mediated glucose transport as a novel target of tributyltin in human embry-  
73 onic carcinoma cells, *Metallomics* 5 (2013) 484–491.  
74 [19] S. Yamada, Y. Kotake, Y. Demizu, M. Kurihara, Y. Sekino, Y. Kanda, NAD-  
75 dependent isocitrate dehydrogenase as a novel target of tributyltin in human  
76 embryonic carcinoma cells, *Sci. Rep.* 4 (2014) 5952.  
77 [20] X. Fan, R. Hussien, G.A. Brooks, H<sub>2</sub>O<sub>2</sub>-induced mitochondrial fragmentation in  
78 C2C12 myocytes, *Free Radic. Biol. Med.* 49 (2010) 1646–1654.  
79 [21] N. Hirata, S. Yamada, T. Shoda, M. Kurihara, Y. Sekino, Y. Kanda, Sphingosine-  
80 1-phosphate promotes expansion of cancer stem cells via S1PR3 by a ligand-  
81 independent Notch activation, *Nat. Commun.* 5 (2014) 4806.  
82 [22] Y. Kanda, T. Hinara, S.W. Kang, Y. Watanabe, Reactive oxygen species mediate  
83 adipocyte differentiation in mesenchymal stem cells, *Life Sci.* 89 (2011)  
250–258.  
84 [23] M.V. Skok, R. Grailhe, F. Agenes, J.P. Changeux, The role of nicotinic receptors  
85 in B-lymphocyte development and activation, *Life Sci.* 80 (2007) 2334–2336.  
86 [24] L.M. Koval, A.S. Zverkova, R. Grailhe, Y.N. Utkin, V.I. Tsetlin, S.V. Komisarenko,  
87 M.V. Skok, Nicotinic acetylcholine receptors alpha4beta2 and alpha7 regulate  
88 myelo- and erythropoiesis within the bone marrow, *Int. J. Biochem. Cell Biol.*  
89 40 (2008) 980–990.  
90 [25] N. He, Z. Wang, Y. Wang, H. Shen, M. Yin, ZY-1, a novel nicotinic analog,  
91 promotes proliferation and migration of adult hippocampal neural stem/  
92 progenitor cells, *Cell Mol. Neurobiol.* 33 (2013) 1149–1157.  
93 [26] C.N. Guo, L. Sun, G.L. Liu, S.J. Zhao, W.W. Liu, Y.B. Zhao, Protective effect of  
94 nicotine on the cultured rat basal forebrain neurons damaged by  $\beta$ -Amyloid  
95 (A $\beta$ )<sub>25–35</sub> protein cytotoxicity, *Eur. Rev. Med. Pharmacol. Sci.* 19 (2015)  
2964–2972.  
96 [27] Q. Liu, B. Zhao, Nicotine attenuates beta-amyloid peptide-induced neurotox-  
97 icity, free radical and calcium accumulation in hippocampal neuronal cultures,  
98 *Br. J. Pharmacol.* 141 (2004) 746–754.  
99 [28] T. Zdravkovic, O. Genbacev, N. LaRocque, M. McMaster, S. Fisher, Human  
100 embryonic stem cells as a model system for studying the effects of smoke  
101 exposure on the embryo, *Reprod. Toxicol.* 26 (2008) 86–93.  
102 [29] E.R. Gritz, V. Baer-Weiss, N.L. Benowitz, M.E. Van VunakisHjarvik, Plasma  
103 nicotine and cotine concentrations in habitual smokeless tobacco users, *Clin.*  
104 *Pharmacol. Ther.* 30 (1981) 201–209.  
105 [30] S. Yamada, Y. Kotake, M. Nakano, Y. Sekino, Y. Kanda, Tributyltin induces  
106 mitochondrial fission through NAD-IDH dependent mitofusin degradation in  
107 human embryonic carcinoma cells, *Metallomics* 7 (2015) 1240–1246.  
108 [31] M. Asanagi, S. Yamada, N. Hirata, H. Itagaki, Y. Kotake, Y. Sekino, Y. Kanda,  
109 Tributyltin induces G2/M cell cycle arrest via NAD<sup>+</sup>-dependent isocitrate  
110 dehydrogenase in human embryonic carcinoma cells, *J. Toxicol. Sci.* (2016) in  
111 press.  
112 [32] V. Choudhary, I. Kaddour-Djebbar, R. Alaisami, M.V. Kumar, W.B. Bollag,  
113 Mitofusin 1 degradation is induced by a disruptor of mitochondrial calcium  
114 homeostasis, CGP37157: a role in apoptosis in prostate cancer cells, *Int. J.*  
115 *Oncol.* 44 (2014) 1767–1773.  
116 [33] M.R. Duchon, Mitochondria and calcium: from cell signalling to cell death,  
117 *J. Physiol.* 529 (2000) 57–68.  
118 [34] N. Demaurex, D. Poberko, M. Frieden, Regulation of plasma membrane cal-  
119 cium fluxes by mitochondria, *Biochim. Biophys. Acta* 1787 (2009) 1383–1394.  
120 [35] A. Tanaka, M.M. Cleland, S. Xu, D.P. Narendra, D.F. Suen, M. Karbowski,  
121 R.J. Youle, Proteasome and p97 mediate mitophagy and degradation of  
122 mitofusins induced by Parkin, *J. Cell Biol.* 191 (2010) 1367–1380.  
123 [36] H. Chen, A. Chomyn, D.C. Chan, Disruption of fusion results in mitochondrial  
124 heterogeneity and dysfunction, *J. Biol. Chem.* 280 (2005) 26185–26192.  
125 [37] W. Yue, Z. Chen, H. Liu, C. Yan, M. Chen, D. Feng, C. Yan, H. Wu, L. Du, Y. Wang,  
126 J. Liu, X. Huang, L. Xia, L. Liu, X. Wang, H. Jin, J. Wang, Z. Song, X. Hao, Q. Chen,  
127 A small natural molecule promotes mitochondrial fusion through inhibition of  
128 the deubiquitinase USP30, *Cell Res.* 24 (2014) 482–496.  
129 [38] S. Lee, F.H. Sterky, A. Mourier, M. Terzioglu, S. Cullheim, L. Olson, N.G. Larsson,  
130 Mitofusin 2 is necessary for striatal axonal projections of midbrain dopamine  
131 neurons, *Hum. Mol. Genet.* 21 (2012) 4827–4835.

Please cite this article in press as: N. Hirata, et al., Nicotine induces mitochondrial fission through mitofusin degradation in human multipotent embryonic carcinoma cells, *Biochemical and Biophysical Research Communications* (2016), <http://dx.doi.org/10.1016/j.bbrc.2016.01.063>